

Chapter 20

Dipolar Spectroscopy – Single-resonance Methods

Peter P. Borbat and Jack H. Freed

Cornell University, Ithaca, NY, USA

20.1	Introduction	425
20.2	Basic Theoretical Aspects of PDS Methods	427
20.3	Double-quantum Coherence EPR, Six-pulse Sequence	434
20.4	Four- and Five-pulse ‘Single-quantum Coherence’ PDS Sequences	438
20.5	Other Single-frequency PDS Methods	446
20.6	2D-FT Orientation-correlation PDS	451
20.7	Relaxation and Instantaneous Diffusion	456
20.8	Conclusions	458
	Acknowledgments	459
	References	459

20.1 INTRODUCTION

Distance measurements on the nanometer scale by pulse EPR have developed into a widely used biophysical method, for which a number of applications and completed studies exist, benefiting particularly the field of structural biology. A key early application

of pulse EPR was concerned with determining the spatial distributions of paramagnetic centers produced in solids by radiolysis. The main approaches to reporting on spatial distributions of radicals in those cases were based on measuring relaxation effects on the primary or stimulated echo, from which concentration-dependent contributions to relaxation could be estimated.^{1,2} The local concentrations affected spectral diffusion in a complicated way due to the inherent complexity of the underlying relaxation processes, but in a more tractable way by the mechanism of ‘instantaneous diffusion’ (ID),^{3–5} which is due to spin echo dephasing caused by the static dipole–dipole interactions among unpaired electron spins of the radicals generated in the radiation tracks. These studies yielded insights into the nature of the dominant solid-state relaxation mechanisms and underlying stochastic processes.^{1,2} Notably, the distinct electron spin-echo envelope modulation (ESEEM) in the primary echo (PE) decay due to the dipolar interactions in spin pairs of SO_4^- radicals produced in single crystal of $\text{K}_2\text{S}_2\text{O}_8$ was reported,^{3,6} showing that the echo decay could be used to determine distances. However, in typical amorphous solids, the echo decays were dominated by phase relaxation and *nuclear* ESEEM,^{7–9} making extracting distance information a very difficult task that was further complicated by long dead times $\approx 0.3\text{--}0.5\ \mu\text{s}$ after the microwave (MW) pulses, leading to a loss of the key part of the signal emanating from the *electron spin dipolar coupling* related ESEEM.

EPR Spectroscopy: Fundamentals and Methods.

Edited by Daniella Goldfarb and Stefan Stoll

© 2018 John Wiley & Sons, Ltd. ISBN: 978-1-119-16299-5

Also published in eMagRes (online edition)

DOI: 10.1002/9780470034590.emrstm1519

Ideally, such experiments should be performed with very strong or ‘hard’ pulses that irradiate the whole spectrum, although the dead time could still be a serious impediment. These issues were overcome when a method originally developed in NMR¹⁰ was implemented in EPR (in 1981)¹¹ as DEER ESE (double electron–electron resonance in electron spin-echo) or simply as DEER (double electron–electron resonance), and since 1998 another name PELDOR (pulsed electron double resonance) has been in use.¹² In this method, the ‘pump’ pulse from an MW power source is applied to affect the amplitude of the electron spin echo formed by the two-pulse ‘detection’ sequence derived from another MW pulse source operating at a different frequency (see Figure 20.1a and Chapter 19).¹¹ The spectral excitations at the two frequencies should not overlap, so the response to the pump pulse is then primarily determined by the electron–electron spin dipolar (as well as electron spin exchange) couplings, producing distinct changes in the amplitude of the spin-echo recorded vs time delay of the pump pulse. The instrumental setup used two independent high-power MW sources, a TWTA (traveling wave tube amplifier) and a magnetron, applied to an MW bimodal cavity resonator housing the sample.

Relaxation effects were small because a fixed delay was used between the detection MW pulses, which were relatively soft and applied at a substantial frequency separation from the pump pulse leading to much reduced nuclear ESEEM.⁸ It was later shown that a single TWTA operating in the linear regime can be used for the task,¹⁴ but before that the single-frequency technique of ‘2+1’ (Figure 20.1a) was introduced and applied to biological systems^{3,15} to overcome the need for two high-power MW sources and associated bimodal resonators and to enable distance measurements on narrow EPR spectra. Subsequently, in another development, the addition of a refocusing pulse to the three-pulse sequence yielded the four-pulse DEER sequence (Figure 20.1b) simplifying technical issues by eliminating the need for the second MW power source.^{16–18} Earlier in an initial study,¹⁹ the fully coherent single-resonance technique of DQC EPR was introduced. It was successfully implemented at K_u band (≈ 17 GHz) as a powerful highly sensitive method offering several distinct advantages based on the use of double-quantum filtering of the dipolar signal as well as the use of ‘constant time’ pulse sequences^{14,20–22} minimizing relaxation effects. It yields clean dipolar signals, zero dead time, and a

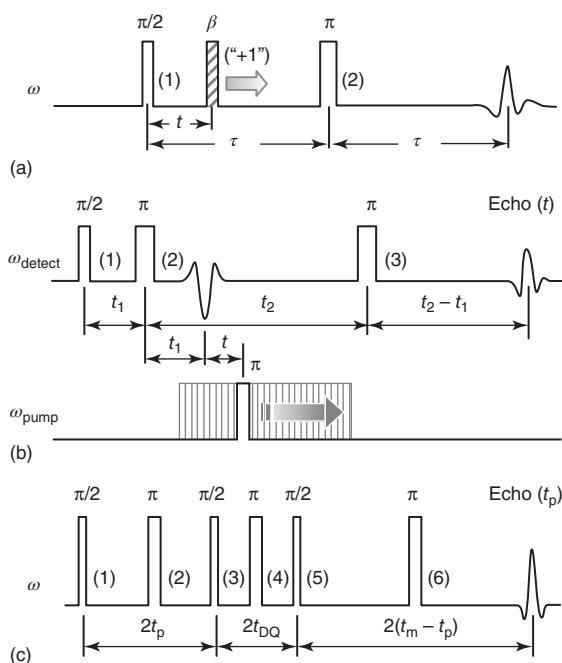


Figure 20.1. The DQC; ‘2+1’, and DEER pulse sequences are shown. (a) The three-pulse DEER (PELDOR), and its analog, ‘2+1’ rely on PE formed by the fixed-position pulses 1 and 2. The dipolar modulation of the echo is produced by letting the spin-flipping ‘pump’ pulse in the middle scan the whole range $(0, \tau)$ between the pulses 1 and 2. In PELDOR, the pump pulse labeled β is at a frequency shifted far enough so as not to affect the spins forming the echo, whereas in ‘2+1’ all the pulses are at (about) the same frequency, so the pulses must not overlap. (b) The four-pulse DEER sequence is formed by adding a π pulse to three-pulse DEER indicated as pulse 3; this converts the PE sequence to a refocused echo. The pump pulse no longer needs to be brought close to pulse 2 as in (a). (c) The six-pulse DQC sequence is much different from the abovementioned sequences by having all six pulses derived from the same coherent source so that each spin participates in ‘pumping’ and detection. The distance between the first pulse and the echo is kept constant, while other pulse positions are varied in a special way to produce the dipolar modulation. (Reproduced with permission from Ref. 13. © Elsevier, 2014)

broad distance range. Since then, there have been two principal *single- and double-resonance techniques* in existence, which are known collectively as *pulse dipolar EPR spectroscopy* (or PDS for short).

PDS has since been enriched with several single- and double-resonance type techniques,^{21–25}

as well as not so distinct types among which RIDME (relaxation-induced dipolar modulation enhancement)^{26,27} recently underwent extensive study and further development.^{28–30} PDS has proved its potential as a sensitive and robust technology to study the structure and function of a broad range of biomolecules^{14,31–35} and a variety of other systems. In the past two decades, there has been a rapid development of newer technical aspects of PDS^{22,24,36–41} including the commercial implementation of four-pulse DEER at X-band (9.4 GHz) and, more recently, the more sensitive Q-band (34 GHz).

20.2 BASIC THEORETICAL ASPECTS OF PDS METHODS

20.2.1 Single and Double Resonance

As we outlined in the Introduction, different PDS methods have been developed to measure electron spin dipolar interactions from which distances can be obtained, to help solve a broad range of molecular structural issues. The whole family of PDS methods continues to expand. This article focuses on *single-resonance techniques* as a subset. As we note in the following section, the distinction between single- and double-resonance experiments is not always obvious. In this context, we cite the definition of double-resonance techniques as given by Slichter in p. 248 of his book⁴² which includes: ‘... *The third category [of double resonance] depends in general on the existence of spin–spin couplings which in many cases must not be unduly obscured by either spin–lattice relaxation or cross-relaxation. We shall therefore call it spin coherence double resonance because it depends on the ability of spins to precess coherently for a sufficient time to reveal the spin–spin splitting. Typically, one here makes use of the fact that when two nuclei [or electron spins] are coupled, changing the spin orientation of one nucleus [or electron spin] changes the precession frequency of the nuclei [or an electron spin] to which it is coupled, so that the second nucleus [spin] can reveal in this way when the first nucleus [spin] is being subjected to a resonant alternating magnetic field. ... Moreover, 2D-FT NMR [or EPR] involving only one nuclear [or electronic] species is not a double-resonance experiment (only one oscillator is used), but it can be conceptually viewed as one in which the ability of a large H_1 ... obviates the necessity of having a*

separate oscillator for each NMR line [each separate portion of the EPR spectrum].’ The reader may note that we introduced EPR parlance in parallel with Slichter’s original quote, as it is equally applicable for EPR and NMR. We already sense a vagueness in trying to define precisely double resonance as just the existence of coherent precession effects due to coupling, which may encompass the whole PDS EPR. However, we do know that there are clearly two distinct approaches to PDS, and having a ‘single oscillator’ is not necessarily the main criterion that sets them apart. The issue of a ‘single-frequency’ experiment is somewhat complicated, particularly so with the advent of modern MW technology where using an NCO (numerically controlled oscillator), one can generate complex time-dependent gigahertz-wide spectrum pulses, which could be polychromatic⁴¹; so we do not necessarily equate single-frequency excitation with single-resonance PDS methods, and we center our discussion around the latter. Our focus here is on ‘genuine’ single-resonance EPR methods, which for the most part employ coherent pulses to control two coupled spins in a coordinated manner and are single-frequency only in that they use a ‘single oscillator’ and are typically best performed with strong B_1 MW fields. Specifically, we would like to mention in this context that such a single-resonance measures coupling that exists in a single group of (electron) spin centers (*A-spins*), which may be of different types but all contribute to the detected signal formed with a sequence of MW pulses, preferably intense ones. All these spins are manipulated by the pulses to transcribe the effect of the coupling onto the evolution of coherences, yielding amplitude modulation of the signal to the maximum effect. On the contrary, in pure double resonance, spins are separated into two groups; one is used to detect the signal, whereas the coupling is revealed typically by using the selective effect of pulse(s) at another frequency or other factors acting on another group of spins, *B-spins* that are dipolar coupled to the *A-spins*. However, double-resonance experiments could in principle be conducted as a single-frequency experiment, for example, ‘light-induced magnetic dipolar spectroscopy’⁴³ and RIDME,^{27,30,44} both are single-frequency experiments, but the evolution of couplings to *B-spins* is measured.

20.2.2 Spin Hamiltonian for Coupled Electron Spins

The theoretical background for PDS has been developed from the concepts utilized in NMR based on the elegant formalism of density matrices, coherences, and product operators (POs) (see Chapter 8).^{45–47} We introduce a simplified form of this here.

For an isolated pair of electron spins, 1 and 2, connected by the vector \mathbf{r}_{12} at angle θ relative to the static field \mathbf{B}_0 , the spin Hamiltonian can be written as

$$\begin{aligned} \hat{H}_0 \equiv \hat{H}_0/\hbar = & (\mu_B/\hbar)\mathbf{B}_0 \cdot \mathbf{g}_1 \cdot \hat{\mathbf{S}}_1 + \hat{\mathbf{I}}_1^{(k)} \cdot \mathbf{A}_1^{(k)} \cdot \hat{\mathbf{S}}_{1z} \\ & + (\mu_B/\hbar)\mathbf{B}_0 \cdot \mathbf{g}_2 \cdot \hat{\mathbf{S}}_2 + \hat{\mathbf{I}}_2^{(l)} \cdot \mathbf{A}_2^{(l)} \cdot \hat{\mathbf{S}}_{2z} \\ & - \gamma_{N1}^{(k)} B_0 \hat{I}_{1z}^{(k)} - \gamma_{N2}^{(l)} B_0 \hat{I}_{2z}^{(l)} + \hat{\mathbf{I}}_1^{(k)} \cdot \mathbf{P}_1^{(k)} \cdot \hat{\mathbf{I}}_1^{(k)} \\ & + \hat{\mathbf{I}}_2^{(l)} \cdot \mathbf{P}_2^{(l)} \cdot \hat{\mathbf{I}}_2^{(l)} + d(3\hat{S}_{1z}\hat{S}_{2z} - \hat{\mathbf{S}}_1 \cdot \hat{\mathbf{S}}_2)/2 \\ & + J(1/2 - 2\hat{\mathbf{S}}_1 \cdot \hat{\mathbf{S}}_2) \end{aligned} \quad (20.1)$$

Here, the first two lines contain electron Zeeman terms for both electron spins and their couplings to their respective sets of nuclei, $\{k\}$ and $\{l\}$ with the summation over these indices implied; $\mathbf{A}_1^{(k)}$, $\mathbf{A}_2^{(l)}$ and \mathbf{g}_1 , \mathbf{g}_2 are the hyperfine (hf) and \mathbf{g} -tensors of the coupled spins both assumed to be spin 1/2. These are followed by nuclear Zeeman and quadrupole terms, which generally cannot be discounted in single-resonance PDS, e.g., due to the development of nuclear ESEEM.^{7–9} However, keeping these terms would be too cumbersome a matter or necessitate numerical treatment. The last two terms describes the electron spin dipolar interaction with the coupling constant $d = \omega_{dd}(1 - 3\cos^2\theta)$ with $\omega_{dd} = \gamma_e^2 \hbar / r_{12}^3$ and the electron exchange with exchange integral $J(r_{12})$. In the dipolar coupling term, only the so-called secular terms A and B were retained, while the nonsecular terms referred to as C, D, E, and F were neglected as is appropriate for high fields.^{4,48} We will simplify the discussion by ignoring other complications and dropping the nuclear spin terms (Zeeman and quadrupole) in line 3. This is the level of approximation used to analyze most PDS experiments, i.e., nitroxides, for which they are insignificant, and also the \mathbf{g} -tensor anisotropy is small. These simplifications will work well for the purpose of this article where we wish to avoid unnecessary complexity. We further simplify with

$$\begin{aligned} \hat{H}_0 = \hat{H}_{12} + \hat{H}_{dd}, \quad \text{where } \hat{H}_{12} = & \Omega_{L1}\hat{S}_{1z} + \Omega_{L2}\hat{S}_{2z} \\ \text{and } \hat{H}_{dd} = & a\hat{S}_{1z}\hat{S}_{2z} + b_{\text{ff}}(\hat{S}_1^+\hat{S}_2^- + \hat{S}_1^-\hat{S}_2^+)/2 \end{aligned} \quad (20.2)$$

Here, \hat{H}_{12} describes the Zeeman and hf terms in lines 1 and 2 of equation (20.1) very simply; this gives us the

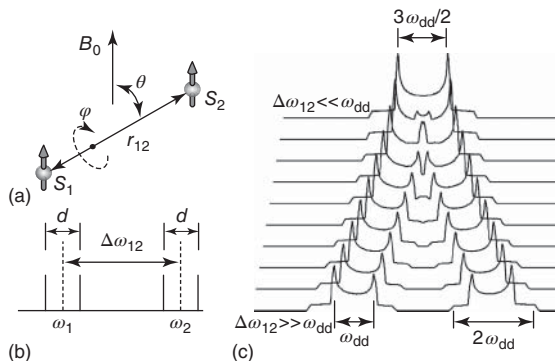


Figure 20.2. (a) Electron spins S_1 and S_2 coupled via the electron spin dipole–dipole interaction. Vector \mathbf{r}_{12} , connecting the spins, is aligned with the z -axis defined in the molecular frame of reference. This frame is given by Euler angles $\Omega = (0, \theta, \varphi)$ relative to the direction of the external magnetic field \mathbf{B}_0 . (b) Dipolar coupling d splits the spectral lines of the electron spins into doublets at offsets $\Delta\omega_1$ and $\Delta\omega_2$. (c) The lineshape in disordered samples resulting from electron spin dipolar couplings for all Ω 's. (Adapted from, Borbat & Freed 2014. (Reproduced with permission from Ref. 22. © Springer, 2014)

frequency spectrum, in the EPR spectral dimension. \hat{H}_{dd} contains the couplings, with $a = d + 2J$ the secular (A) part and $b_{\text{ff}} = -d/2 + 2J$, the pseudosecular (or flip-flop, B) part. In the frame of reference rotating with the frequency ω_0 of the applied MW field (the rotating frame, for short), we replace the Larmor frequencies Ω_{Lk} with their offsets $\Delta\omega_k = \Omega_{Lk} - \omega_0$. The dipolar coupling term in equation (20.2) splits each of the two resonant lines at $\Delta\omega_1$ and $\Delta\omega_2$ into two lines separated by d for $\omega_{dd} \ll \Delta\omega_{12} = |\Delta\omega_1 - \Delta\omega_2|$; but by $3d/2$ in the opposite case of $\omega_{dd} \gg \Delta\omega_{12}$ (Figure 20.2). In samples with an isotropic distribution of orientations, the dipolar lineshape averaged over all orientations takes the form of a Pake doublet^{8,49,50} in both cases. In intermediate cases, when $\omega_{dd} \approx \Delta\omega_{12}$, the lineshape is more complex and can be obtained numerically.

20.2.3 Density Operator and Coherences

The ensemble of electron spin pairs in a PDS sample is defined by the density operator (see Chapter 8). At equilibrium temperature T , it is given by⁴

$$\hat{\sigma}_{\text{eq}} = \exp(-\hat{H}_0/kT)/\text{tr}(\exp(-\hat{H}_0/kT)) \quad (20.3)$$

where $\hat{H}_0 = \hbar\hat{H}_0$ is generally a many-body spin-Hamiltonian, which for a spin pair is given by equation (20.2). In a magnetically dilute sample, the magnetic interaction of all the spins pairs in the sample is described by the secular dipolar Hamiltonian.⁴⁸ The intramolecular couplings within each spin pair are dominant in PDS, so that we omit for now intermolecular interactions with the electron spins on surrounding molecules, but we introduce them later, as needed. The equilibrium density operator at high magnetic field and high temperature for a spin pair can be reduced to the form of just a series expansion of the exponential operator where in lowest order⁴⁸

$$\hat{\sigma}_0 = -(\hat{S}_{1z} + \hat{S}_{2z}) \quad (20.4)$$

(where we ignore extra constants). The equivalent density matrix σ_0 at equilibrium contains only diagonal elements corresponding to energy levels with equilibrium populations. In a perturbed system, e.g., in the presence of resonant MW radiation (or by a light pulse), the populations are no longer at equilibrium, and there are off-diagonal elements (or coherences) representing the transitions.^{45,51,52} They oscillate with their transition frequencies corresponding to the connected levels and coherence orders, \bar{p} , particularly important for larger spin systems. The order depends on the number of single-spin transitions involved in a (multiquantum) transition and is characterized by the change $\Delta\bar{p}$ in magnetic quantum number, e.g., for a single spin $\Delta\bar{p} = \pm 1$ for single-quantum transitions.

20.2.4 Evolution of Coupled Spins

PDS is a pulse EPR experiment, i.e., it is conducted by subjecting the equilibrium spin system to a sequence of MW pulses separated by periods of free evolution and after a certain time detecting the precessing magnetization $M_y(t)$. The initial transverse magnetization is usually created by a $(\pi/2)_x$ pulse from the equilibrium state of equation (20.4), yielding $\hat{\sigma}_{12}(0+) = \hat{S}_{1y} + \hat{S}_{2y}$. Then the free precession of spins proceeds with their (Larmor) frequency offsets $\Delta\omega_k$, $k = 1, 2$. With each precessing spin, there are associated coherences $\bar{p} = \pm 1$ evolving as $\exp(\mp i\Delta\omega_k t)$. The detected signal is given by $M_y(t) \propto -2\text{Im}\{\text{tr}(\hat{\sigma}_{12}(t)\hat{S}^+)/\text{tr}(\hat{S}^-\hat{S}^+)\}$ where $\hat{S}^\pm = \hat{S}_1^\pm + \hat{S}_2^\pm$. (The denominator normalizes $M_y(0)$ to unity). The observable \hat{S}_x and \hat{S}_y components in $\hat{\sigma}_{12}(t)$ both contain the \hat{S}^- coherence. In solids, nearly always the spin-echo is detected (see Chapter 11).

The spin dynamics of the ensemble of noninteracting spin pairs, leading to the echo, is described by the Liouville–von-Neumann equation

$$\frac{d\hat{\sigma}_{12}}{dt} = -i[\hat{H}, \hat{\sigma}_{12}] \quad (20.5)$$

which for the time-independent \hat{H} , e.g., \hat{H}_0 of equation (20.2) gives the free evolution of $\hat{\sigma}_{12}(t)$. The solution then is expressed as a unitary transformation of $\hat{\sigma}_{12}(0) = \hat{\sigma}_0$

$$\hat{\sigma}_{12}(t) = \exp(-i\hat{H}t)\hat{\sigma}_{12}(0)\exp(i\hat{H}t) \quad (20.6)$$

The pulse experiment gives the combined effect of a sequence of pulse propagators separated by the periods of free evolution described by the free evolution propagator $\hat{U}(t) = \exp(-i\hat{H}_0 t)$, during which coherence orders and polarizations are preserved in the absence of relaxation. The free evolution of each matrix element is determined by its transition frequency and coherence order. As the density operator is evolved by the pulse sequence, any element of the density matrix can be populated or changed by the pulses.

In the presence of the n th MW pulse, \hat{H} becomes $\hat{H}_n = \hat{H}_0 + \hat{H}_{1n}$, where n numbers the pulses. In the rotating frame, the pulse spin-Hamiltonian is

$$\begin{aligned} \hat{H}_{1n} &= \omega_{1n}(\hat{S}^+ e^{-i\varphi_n} + \hat{S}^- e^{i\varphi_n})/2 \\ &= \omega_{1n}(\hat{S}_x \cos \varphi_n + \hat{S}_y \sin \varphi_n) \end{aligned} \quad (20.7)$$

The n th pulse is characterized by its nutation frequency $\omega_{1n} = -\gamma_e B_{1n}$, duration Δt_n , and phase φ_n . The action of a pulse is then described as a rotation. (If the n th pulse frequency is shifted by $\Delta\omega_{0n}$, equation (20.7) may need to add $\Delta\omega_{0n} t$ to φ_n or, as usually done, to change ω_0 by $\Delta\omega_0$ in our treatment). In the more complicated case of a time dependence in the rotating frame \hat{H}_{1n} such as encountered with shaped pulses⁵³ (see Chapter 21), the pulse amplitude and phase temporal envelopes can be approximated by a sequence of discrete time-independent \hat{H}_{1n} and the complex evolution is obtained by integrating the sequence of small-angle rotations. For constant ω_{1n} during the pulse and the spins at $\Delta\omega = 0$ equation (20.6) represents rotation by angle $\beta_n = \omega_{1n} \Delta t_n$, for $\Delta\omega \neq 0$ there are off-resonance effects⁸ (see Chapter 11). We will avoid unnecessary complications by assuming hard (nearly infinite B_1) pulses, except as noted. The finite pulses in PDS can be treated using existing approaches.²¹

The evolution of coherences is often depicted as a coherence pathway transfer (CPT) chart where pulses

change coherence orders. A perfect π -pulse changes signs of coherence orders as $\bar{p} \rightarrow -\bar{p}$, which can be viewed as time reversal that enables refocusing. It also inverts polarizations represented by polarization operators, $\hat{S}_k^\alpha \equiv \hat{E}_k/2 + \hat{S}_{kz}$ and $\hat{S}_k^\beta \equiv \hat{E}_k/2 - \hat{S}_{kz}$ as $\hat{S}_k^\alpha \leftrightarrow \hat{S}_k^\beta$, which is essential for PDS. (Here, \hat{E}_k is the identity operator for spin k). An arbitrary pulse can change a given coherence order \bar{p} to any and all available orders. For a single spin, it can change coherence order $\pm 1 \leftrightarrow 0$, refocus $\pm 1 \leftrightarrow \mp 1$, or invert population. A $\pi/2$ pulse, for example, can refocus (or flip) half of the spins, i.e., $\hat{S}^+ \xrightarrow{(\pi/2)_x} (\hat{S}^+ + \hat{S}^-)/2 + i\hat{S}_z$, producing both coherence orders and z -magnetization (which we will refer to as ‘coherence order 0’). The picture becomes richer for coupled spins where the coupling can be refocused, higher orders with $|\bar{p}| > 1$ may occur, and coherence transfer (CT)⁴⁵ between spins is possible.

Relaxation effects are very important and could be included phenomenologically¹⁹ using spin–lattice and spin–spin relaxation times T_1 , T_2 , and T_m denoting the phase memory time. If relaxation needs to be considered rigorously, one should resort to the superoperator form solving the stochastic Liouville equation (SLE) $\hat{\sigma}(t) = -(i/\hbar)\hat{L}\hat{\sigma}(t) + \hat{I}(\hat{\sigma}(t) - \hat{\sigma}_{\text{eq}})$, which includes the Liouville, $\hat{L}\hat{\sigma} = \hat{H}\hat{\sigma} - \hat{\sigma}\hat{H}$, and relaxation \hat{I} superoperators, and is generally a many-body problem.^{45,54,55} We do not need to bring the SLE into this article, as relaxation will only be treated phenomenologically.

20.2.5 Product Operators

Here, we are mostly concerned about PDS based on *coherent single-resonance* methods. Our simplified treatment is conducted based on the spin Hamiltonian of equation (20.2). A formal description of PDS uses the density operator, whose time evolution is followed by solving equation (20.5) in the rotating frame using propagators based on respective spin-Hamiltonians \hat{H}_0 and \hat{H}_n for free evolution and pulses, usually assumed to be hard (see Section 20.2.4). This issue is often simplified by employing the PO method (see Chapter 8),^{45,46,52,56,57} (although a numerical treatment is hard to avoid in EPR). Throughout the text, we assume $J=0$ and weak dipolar coupling by dropping the flip-flop terms (i.e., $b_{\text{ff}}=0$), but one may consider them where this is needed, for which

a modified PO treatment exists.²¹ That is, we use $\hat{H}_{\text{dd}} = a\hat{S}_{1z}\hat{S}_{2z}$. In this case, \hat{H}_{dd} and the rest of \hat{H}_0 in equation (20.2) commute, which enables us to use the PO method in its basic form originally developed for NMR.

In the PO method, the density operator is constructed using a suitable operator basis.⁴⁵ For a spin pair, the density operator $\hat{\sigma}_{12}$ may be expressed in the operator basis taken as a direct product of the individual density operator bases for $\hat{\sigma}_1$ and $\hat{\sigma}_2$ for each spin, e.g., taken as the Cartesian $\hat{E}_k/2, \hat{S}_{kz}, \hat{S}_{kx}, \hat{S}_{ky}$ basis, where $k=1, 2$.^{45,47} To follow the evolution of coherences, we prefer a modified spherical basis $\hat{E}_k/2, \hat{S}_{kz}, \hat{S}_k^+, \hat{S}_k^-$,^{21,52} where $\hat{S}_k^\pm = \hat{S}_{kx} + i\hat{S}_{ky}$ are raising and lowering operators. The direct product basis contains a set of 16 operators making a complete set of 15 basis operators plus the identity operator. The polarization and coherence states are represented, respectively, by diagonal and off-diagonal elements in the matrix representation of the two-spin density operator. Off-diagonal elements correspond to $\bar{p}=0, \pm 1, \pm 2$. The diagonal elements correspond to $\bar{p}=0$. Polarization states are represented by the POs $\hat{S}_{1z}, \hat{S}_{2z}, 2\hat{S}_{1z}\hat{S}_{2z}$ with the first two related to populations, whereas the last represents ‘dipolar order’ $\hat{P}_{12} = 2\hat{S}_{1z}\hat{S}_{2z}$, which can be created by pulses or exists in the expansion of the density operator at high fields and low temperature, where the spin polarization is large. Or it could be produced in a reaction, such as initiated by a light pulse.^{58,59}

We will need to follow coherences to fully describe the pulse sequences: single-quantum in-phase (I^\pm); single-quantum antiphase (A^\pm); and double-quantum (DQ^\pm). Their respective POs are as follows:

$$\begin{aligned} \hat{I}_1^\pm &= \hat{S}_1^\pm, \quad \hat{I}_2^\pm = \hat{S}_2^\pm; \quad \hat{A}_1^\pm = 2\hat{S}_1^\pm\hat{S}_{2z}, \quad \hat{A}_2^\pm \\ &= 2\hat{S}_2^\pm\hat{S}_{1z}; \quad DQ^\pm = \hat{S}_1^\pm\hat{S}_2^\pm \end{aligned} \quad (20.8)$$

20.2.6 Evolution of SQC

As \hat{H}_{12} and \hat{H}_{dd} commute at the level of approximation used here, the evolution of coherences due to offset and coupling can be treated independently. The POs defined in Cartesian form^{45–47} are convenient for treatment of the pulses, while the spherical PO form is usually better for treatment of the free evolution and following the coherence orders. In both cases, the respective propagators for \hat{H}_{12} and \hat{H}_{dd} expressed using a PO basis are independently applied to describe the

evolution of the density operator $\hat{\sigma}_{12}$. The free evolution may thus be conveniently followed in the spherical basis. It is given as:

$$\hat{S}_k^\pm \xrightarrow{\hat{H}_{12}t} \hat{S}_k^\pm \exp(\mp i\Delta\omega_k t) \quad (20.9)$$

$$\hat{S}_k^\pm \xrightarrow{\hat{H}_{dd}t} \hat{S}_k^\pm (\cos at/2 \mp i2\hat{S}_{jz} \sin at/2) \quad (20.10)$$

where the subscript $j \neq k$ is for the other spin ($j, k = 1, 2$) and a is their coupling. The \hat{S}_k^\pm evolves due to \hat{H}_{12} as given by equation (20.9), describing two first-order coherences ($\bar{p} = \pm 1$) associated with precession at offset $\Delta\omega_k$. We characterize this evolution by the phase Φ_{off} or ‘offset phase’, with time derivative $\dot{\Phi}_{\text{off}} = \Delta\omega_k(t)\bar{p}$. The evolution due to \hat{H}_{dd} in equation (20.10) describes the evolution as interconversion between two terms of which the first is observable, whereas the second term, $2\hat{S}_k^\pm \hat{S}_{nz}$, describes the ‘antiphase’ order that develops between the two spins and is not directly observable, as its trace product with \hat{S}_k^\pm vanishes. (Such coherences represent antiphase doublets in NMR,⁴⁵ but discussion of such details is not needed here.) We can describe this evolution by the more difficult to track ‘dipolar phase’ Φ_{dip} for which $\dot{\Phi}_{\text{dip}} = \bar{p}\bar{z}(a/2)$, where \bar{z} is +1 for \hat{S}_n^α and –1 for \hat{S}_n^β . (Note, it is not the sign of \bar{z} but its change that matters, as the in-phase component in $\cos \Phi_{\text{dip}}$ is detected. We can select \hat{S}_n^α as initial condition before the start of the pulse sequence.) Both phases describe evolution that can be reversed, so that the conditions of offset or coupling refocusing could be achieved.

A real (arbitrary) pulse can produce all possible coherence orders available for the observed spins, yielding a number of coherence pathways, from which the pathway of interest is then selected by performing phase cycling and by restricting some interpulse intervals.⁸ Each pulse acting along this pathway may produce alternative (reversed/unreversed) routes for $\Phi_{\text{dip}}(t)$ for a fraction of the spins, leading to a set of different $\Phi_{\text{dip}}(t)$ ’s, which we will call ‘dipolar pathways’ or more distinctly ‘trajectories’. Such dynamics is accounted for automatically by the PO for ideal hard pulses, as well as in a rigorous density matrix treatment. For arbitrary pulses, the standard PO method should be applied with consideration of such effects. In double resonance, in particular, the effect of pulses on the B-spins should account for what is the arbitrary nature of the pulse, which can be done first by calculating the probability p to flip this spin and then use it with equation (20.10) cast into a

form conducive to the analysis of dipolar phase evolution.

$$\hat{S}_1^\pm \xrightarrow{H_{dd}t} \hat{S}_1^\pm (c_t \mp i s_t 2\hat{S}_{2z}) \equiv \hat{S}_1^\pm \hat{D}_{\pm t} \quad (20.11)$$

where $c_t = \cos(at/2)$ and $s_t = \sin(at/2)$. The propagators $\hat{D}_{\pm t}$ (or $\hat{D}(\pm t)$) can be used to derive trajectories Φ_{dip} for a coherence pathway of interest taking into account that \hat{D}_t has the following convenient properties:

$$\begin{aligned} \hat{D}_t &\xrightarrow{\hat{H}_{nc}} q_{kn}^{(c)} \hat{D}_t + p_{kn}^{(c)} \hat{D}_t^* \\ \hat{D}_t^* &= \hat{D}_{-t}, \quad \hat{D}_{t_1+t_2} = \hat{D}_{t_1} \hat{D}_{t_2} \end{aligned} \quad (20.12)$$

where $p_{kn}^{(c)}$ is the probability for pulse n to change polarization state of spin k (‘flip’ it). In equation (20.12), $q_{kn}^{(c)}$ is the probability for the spin to be unaffected by the pulse. Superscript $c = (A, B)$ denotes the frequency at which the pulse is applied in cases of chirp pulses or DEER, i.e., to A or B spins. Then, it is straightforward to evolve the pulse sequence along the pathway, but many trajectories with different amplitudes and timing variables may be generated. For example, there are four distinct trajectories with time dependence in four-pulse DEER or refocused ‘2+1’, three of which are unwanted. This is also the case with DEER when there is more than one pump pulse.^{22,24} It is also a major problem with single-resonance and single-frequency methods in general.

20.2.7 Refocusing Offsets and Coupling

We showed above with POs the free evolution for a spin pair; now the effect of pulses should be elucidated. We consider two coupled spins A and B at Larmor frequencies ω_A and ω_B with offsets $\Delta\omega_A$ and $\Delta\omega_B$. (We will denote the A- and B-spin operators (and offsets) by subscript $k = 1, 2$ for consistency throughout the chapter.) In single-resonance experiments ($\omega_A \approx \omega_B$), both spins are assumed to be at or near the detection frequency ω_A , and for double resonance, spin 1 is an A spin. As we detect an echo, refocusing by π -pulse(s) is necessary. The simplest refocusing sequence is an echo refocusing sequence $\tau-\pi-\tau$ or ‘sandwich’ corresponding to a PE (see Chapter 11). With POs, the refocusing is expressed as:

$$\begin{aligned} S_k^+ &\xrightarrow{H_0\tau} S_k^+ \exp(-i\Delta\omega_k \tau) \\ &\xrightarrow{\pi} S_k^- \exp(-i\Delta\omega_k \tau) \xrightarrow{H_0t} S_k^- \exp(-i\Delta\omega_k(\tau-t)) \end{aligned} \quad (20.13)$$

At $t = \tau$, the offset refocuses, and an echo is formed. Equation (20.13) describes the coherence pathway $+1 \rightarrow -1$. In Figure 20.3, we show three principal cases when π -pulses act on one of the two spins or both. The refocusing of an A spin is performed in panels (a) and (c); the pulse at ω_B in (b, c) affects spin 1 at ω_A indirectly through the evolution of the coupling. The effect of a pulse on dipolar evolution occurs through the antiphase $2\hat{S}_1^+ \hat{S}_{2z}$ term in equation (20.10). In panel (a), the pulse at ω_A flips spin A, refocusing both the echo, according to equation (20.13), and the coupling by the refocusing $2\hat{S}_1^+ \hat{S}_{2z}$ to $2\hat{S}_1^- \hat{S}_{2z}$. The coupling is refocused in panel (b) but, in this case, through population inversion $\hat{S}_{2z} \rightarrow -\hat{S}_{2z}$.

We can treat both cases in panels (a) and (c) simultaneously by introducing the probability p to flip the B-spin. Then, $q = 1 - p$ is the probability not to flip. We follow the evolution starting with \hat{S}_1^+ ,

$$\begin{aligned} \hat{S}_1^+ &\xrightarrow{H_{\text{dd}}\tau} \hat{S}_1^+(c_\tau - i2\hat{S}_{2z}s_\tau) \\ &\xrightarrow{(\pi)} \hat{S}_1^-[(q+p)c_\tau - i2(q-p)\hat{S}_{2z}s_\tau] \\ &\xrightarrow{H_{\text{dd}}t} \hat{S}_1^-[q(c_\tau - i2\hat{S}_{2z}s_\tau) \\ &\quad + p(c_\tau + i2\hat{S}_{2z}s_\tau)](c_t + i2\hat{S}_{2z}s_t) \\ &= \hat{S}_1^-[q(c_{\tau-t} - i2\hat{S}_{2z}s_{\tau-t}) + p(c_{\tau+t} + i2\hat{S}_{2z}s_{\tau+t})] \end{aligned} \quad (20.14)$$

For $t = \tau$, the result is $\hat{S}_1^-[q + p(c_{2\tau} + i2\hat{S}_{2z}s_{2\tau})]$, which for $p = 1$, corresponding to hard π -pulse at ω_B , is $\hat{S}_1^-(c_{2\tau} + i2\hat{S}_{2z}s_{2\tau})$, i.e., $\Phi_{\text{dip}}(t)$, unaffected by the π -pulse, is evolving as $at/2$. For $p = 0$, equivalent to the absence of any pulse resonant with B-spin, we have just \hat{S}_1^- corresponding to complete refocusing.

Panel (b) has a π -pulse only at ω_B and it shows that Φ_{dip} is refocused (reverses direction) by the pulse. This sets the stage for evolving dipolar coupling by moving the pulse(s) at ω_B along the time axis while keeping the echo-forming ‘observe’ pulse sequence at A invariant. With the pulse assets of Figure 20.3, one can realize three-pulse DEER by combining panels (a) and (b). The sequence of panel (c), which actually best represents the single-resonance case, i.e., $\omega_A \approx \omega_B$ (with spin resonance offsets denoted $\Delta\omega_1$ and $\Delta\omega_2$ in this article), does not provide any means to evolve the coupling other than to expand the sandwich starting from its minimal width, limited by the dead time in practice. There are known issues with three-pulse DEER caused by pulse overlap, so it was modified by adding one more sandwich^{16,18} to produce a refocused echo (RE) (see Chapter 19). A similar approach based on

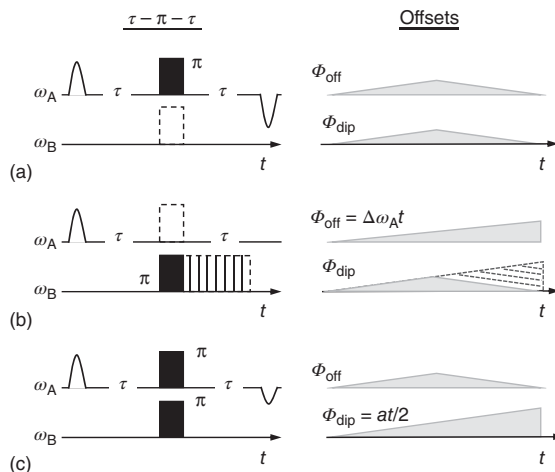


Figure 20.3. Coherence evolution of two coupled spins in the echo refocusing (or ‘spin-echo’) pulse sequence (or ‘sandwich’ for short) $\tau - \pi - \tau$. The pair of coupled spins, A (at ω_A) and B (at ω_B), is characterized by their Larmor frequency offsets $\Delta\omega_A$ and $\Delta\omega_B$ and their coupling a . Here, we are interested in refocusing the coherence for A-spins. In the absence of a pulse, first-order coherence phases evolve (from echo at $t = 0$) as $\Phi_{\text{off}} = \Delta\omega_A t$ due to offsets and $\Phi_{\text{dip}} = at/2$ due to coupling. (a) Refocusing π pulse is applied at the offset $\Delta\omega_A$ to flip an A spin. Both frequency offset and coupling are refocused, and both phases are zero at $t = 2\tau$, where the inverted echo is observed. This is complete reversal of the time evolution; that is, coherence amplitude at $t = 0$ fully recovers at $t = 2\tau$ for any a . (b) If the pulse is applied at $\Delta\omega_B$, there is no offset refocusing, but the coupling is refocused as shown. Refocusing the offset of spin A then requires applying additional π pulses outside of the sandwich. However, the pulse at ω_B is free to move along the time axis without any effect on offsets at $\Delta\omega_A$, thereby allowing one to control refocusing of Φ_{dip} , e.g., delaying it as indicated by dashed lines. This is what is used in double resonance. (c) The π -pulses flip both spins. (It can be just one pulse if $\omega_A \approx \omega_B$.) The offsets are refocused, but the coupling is not, leading to incomplete reversal of the evolution. The first-order coherence amplitude V_0 (e.g., spin echo) at time $t = 0$ will be $V_0 \cos a\tau$ at time $t = 2\tau$, so it does not refocus in full for all a 's and will decay for a distribution in a . The evolution is characterized by linear ‘dipolar phase’ $\Phi_{\text{dip}} = at/2$. This is the case that single-resonance deals with

RE can be applied to the single-frequency case. This we show in Figure 20.4(a). The four-pulse DEER sequence is depicted for comparison in panel (b) together with its Φ_{off} and Φ_{dip} evolution graphs. The particular timing $\tau - 2\tau - \tau$ -echo¹⁶ was not the most efficient to evolve couplings; therefore, the timing was changed

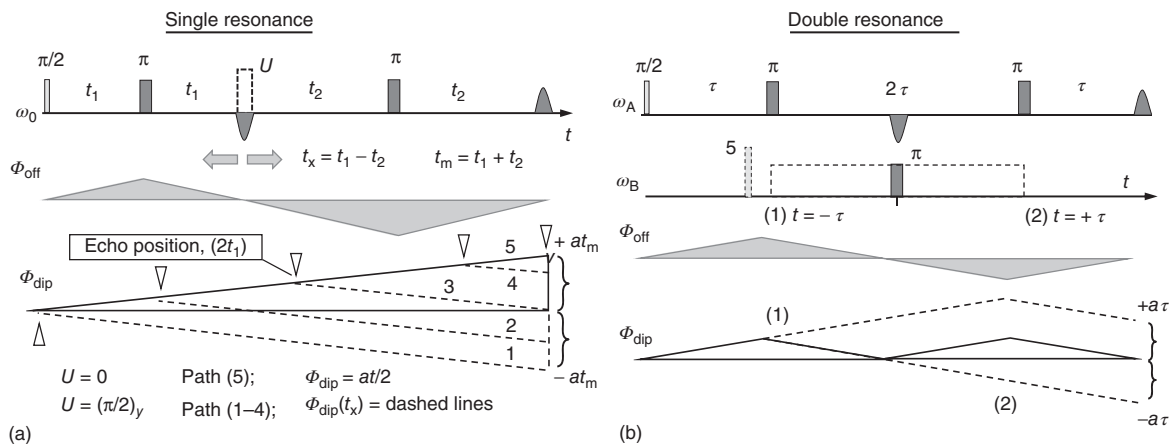


Figure 20.4. Two principal PDS schemes based on RE. (a) In a single-resonance sequence based on a sequence of two echo sandwiches, the evolution of the coupling is not refocused by any of the π pulses; thus, the progress of the dipolar phase Φ_{dip} (line 5 in a) is $at/2$, reaching at_m at the RE formed at $2t_m$. Here, Φ_{dip} does not depend on $t_x = t_1 - t_2$, so no evolution can be produced at constant t_m by varying t_1 . A more complex spin manipulation, such as by a propagator \hat{U} inserted between the refocusing sequences can change this picture by modifying one or both of the first-order coherences (i.e., of in- and antiphase). For example, just a single $(\pi/2)_y$ negates the antiphase term, hence refocusing the coupling. The envelopes of Φ_{dip} are shown for five positions of $(\pi/2)_y$, and echo at $2t_1$, as indicated by the wedges. Lines 1–4 are all different, leading for t_x in $[-t_m, t_m]$ to the maximum range of change at_m possible for $|\Phi_{\text{dip}}|$ over $2t_m$ evolution period. Other forms of propagator \hat{U} are discussed in the following sections. (b) Double-resonance approach to the RE sequence. The in-phase coherence created by the initiating $\pi/2$ pulse is refocused in each of the two sandwiches, which, in this example, have equal durations. The π pulse at frequency ω_B can be applied at any time point, unlike in a, but does not need to be outside points 1 and 2. As it moves between the two π -pulses at $\Delta\omega_A$, Φ_{dip} changes from $-a\tau$ to $a\tau$, crossing the coupling refocusing point in the middle at $t=0$. When π pulses at the two frequencies coincide, evolution does not reverse (dashed lines 1 and 2). The range of $|\Phi_{\text{dip}}|$ is $a\tau$, i.e., only half that shown in a for $t_m = 2\tau$. Making this pulse sequence asymmetric, as in a by making $t_1 \ll t_2$; or adding a π pulse (5) at $\Delta\omega_B$ and position near 1 or 2 recovers the full range of $|\Phi_{\text{dip}}|$ by shifting the range of Φ_{dip} (4τ) to be nearly completely above or below zero

to $t_1 - (t_1 + t_2) - t_2 - \text{echo}$, with $t_1 \ll t_2$.⁶⁰ In a different approach, another pulse was added for the B-spins, creating the DEER-5 method.²⁴ This demonstrates the flexibility of PDS based on double resonance.

We will use two notations for the timing in RE-based constant-time pulse sequences. We will use $2t_m$ for the length of a sequence (from the beginning to the echo) and t_1, t_2 for the two sandwiches in RE (i.e., $t_1 - \pi - t_1, t_2 - \pi - t_2$). Thus $t_1 + t_2 = t_m$. We will also use t_p for t_1 , while $t_m - t_p$ will be used for t_2 to emphasize the constant-time sequence. Finally, we introduce the dipolar evolution variable $t_x = t_1 - t_2 = 2t_p - t_m$. (We also used t_x for $-t_x$ in the past.²¹) The range of change for $t_x = [-t_m, t_m]$. This is the preferred (constant-time) way to record evolution with single-resonance pulse sequences, which we detail in the following sections.

It is very clear from Figure 20.4 that there is no evolution of dipolar coupling in RE as a function of t_x .

The number of refocusing pulses can be any, but the result is the same, Φ_{dip} evolves as $at/2$ reaching at_m at the echo. To see this, the evolution can be expressed as follows. In the first sandwich, the evolution (for spin 1) proceeds according to:

$$\begin{aligned} \hat{S}_1^\pm &\xrightarrow{\hat{H}_{\text{dd}}\tau} \hat{S}_1^\pm(c_\tau \mp i2\hat{S}_{2z}^s s_\tau) \xrightarrow{(\pi)} \hat{S}_1^\mp(c_\tau \pm i2\hat{S}_{2z}^s s_\tau) \\ &\xrightarrow{\hat{H}_{\text{dd}}t} \hat{S}_1^\mp(c_\tau \pm i2\hat{S}_{2z}^s s_\tau)(c_t \pm i2\hat{S}_{2z}^s s_t) \\ &= \hat{S}_1^\mp(c_{\tau+t} \pm i2\hat{S}_{2z}^s s_{\tau+t}) \rightarrow \hat{S}_1^\mp(c_{2\tau} \pm i2\hat{S}_{2z}^s s_{2\tau}) \end{aligned} \quad (20.15)$$

(For spin 2, the result $\hat{S}_2^\pm = \hat{S}_2^\mp(c_{2\tau} \pm i2\hat{S}_{1z}^s s_{2\tau})$ is obtained by swapping the subscripts.) Note that we omitted evolution due to offsets in equation (20.15) as they are refocused in equation (20.13) for $t = \tau$. (They should be retained, however, if one is considering 2D experiments that rely on the time variable $\delta t = t - \tau$.) Having obtained the evolution for \hat{S}_1^\mp and \hat{S}_2^\pm at 2τ , we

then switch to Cartesian PO's

$$\begin{aligned}\hat{S}_{1y} &= (\hat{S}_1^+ - \hat{S}_1^-)/2i = [\hat{S}_1^-(c_{2\tau} + i2\hat{S}_{2z}s_{2\tau}) \\ &- \hat{S}_1^+(c_{2\tau} - i2\hat{S}_{2z}s_{2\tau})]/2i = -\hat{S}_{1y}c_{2\tau} + i2\hat{S}_{1x}\hat{S}_{2z}s_{2\tau}\end{aligned}\quad (20.16)$$

Similar to equation (20.15), $\hat{S}_{2y} = -\hat{S}_{2y}c_{2\tau} + i2\hat{S}_{2x}\hat{S}_{1z}s_{2\tau}$ and finally for $(\hat{S}_{1y} + \hat{S}_{2y})$,

$$-(\hat{S}_{1y} + \hat{S}_{2y})c_{2\tau} + i(2\hat{S}_{1x}\hat{S}_{2z} + 2\hat{S}_{2x}\hat{S}_{1z})s_{2\tau}\quad (20.17)$$

or simply $\cos at$ for evolution. The evolution of coupling in an RE can be described as follows. We will track spin 1, then after the first sandwich $(t_1 - \pi - t_1)$ according to equation (20.16), there is in-phase coherence $\hat{I}_1(t_1) = -\hat{S}_{1y} \cos at_1$ and antiphase coherence $\hat{A}_1(t_1) = 2\hat{S}_{1x}\hat{S}_{2z} \sin at_1$. After the second sandwich, these terms evolve into detectable in-phase terms as

$$\begin{aligned}\hat{I}_1(t_1) + \hat{A}_1(t_1) &\rightarrow \hat{I}_1(t_1 + t_2) \\ &= \hat{S}_{1y}(\cos at_1 \cos at_2 - \sin at_1 \sin at_2)\end{aligned}\quad (20.18)$$

The term in cosines can be viewed as the evolution path $\hat{I}_1(0) \rightarrow \hat{I}_1(t_1) \rightarrow \hat{I}_1(t_1 + t_2)$, while that in sines as $\hat{I}_1(0) \rightarrow \hat{A}_1(t_1) \rightarrow \hat{I}_1(t_1 + t_2)$. The outcome is $\hat{S}_{1y} \cos at_m$, the same as in the case with PE; the only dipolar evolution possible is that by varying t_m , starting from the end of the dead time, t_{\min} . To overcome this trend, we need somehow to refocus Φ_{dip} , a task that unlike in double resonance just cannot be accomplished with π -pulses. However, this can be done, for example, by inserting between the sandwiches a propagator \hat{U} , which is able to refocus directly or indirectly, as we will soon show. \hat{U} will be allowed to evolve coherence orders 0 and ± 2 . It may contain several pulses, may have a long duration, and can make use of phase relaxation or of any other spin manipulation. We describe its transfer properties in an arbitrary manner as $C_1\hat{I}_k + C_A\hat{A}_k$, where $k = 1, 2$ numbers the two spins and $|C_{I(A)}| \leq 1$. As the evolution is for $\bar{p} = 0, \pm 2$ orders, no dipolar evolution takes place and the (stored) dipolar phase is carried through. Relaxation can render zero either C_1 or C_A , as we will see. (Phase cycling can produce an equivalent result.) Then, equation (20.18) transforms to

$$\begin{aligned}\hat{I}_1(t_1) + \hat{A}_1(t_1) &\xrightarrow{\hat{U}} C_1\hat{I}_1(t_1) + C_A\hat{A}_1(t_1) \\ &\xrightarrow{t_2} \hat{S}_{1y}(C_1 \cos at_1 \cos at_2 - C_A \sin at_1 \sin at_2) \\ &= \hat{S}_{1y}[(C_1 + C_A) \cos at_m + (C_1 - C_A) \sin at_x]\end{aligned}\quad (20.19)$$

If $C_1 = -C_A$, only $\cos at_x$ remains; this is the case of coupling completely being refocused at $t_x = 0$. This

can be achieved by solid-echo refocusing,⁶¹ i.e., applying $\hat{U} = (\pi/2)_y$ refocuses the coupling according to

$$\begin{aligned}&-(\hat{S}_{1y} + \hat{S}_{2y})c_{2t_1} + i(2\hat{S}_{1x}\hat{S}_{2z} + 2\hat{S}_{2x}\hat{S}_{1z})s_{2t_1} \\ &\xrightarrow{(\pi/2)_y} -(\hat{S}_{1y} + \hat{S}_{2y})c_{2t_1} - i(2\hat{S}_{2x}\hat{S}_{1z} + 2\hat{S}_{1x}\hat{S}_{2z})s_{2t_1}\end{aligned}\quad (20.20)$$

This is equivalent to $t_1 \rightarrow -t_1$ in $\sin at_p$, i.e., time reversal, but it comes at the expense of swapping antiphase coherences of the spins. A $(\pi/2)_x$ pulse instead stores \hat{S}_{ky} as $-\hat{S}_{kz}$, plus it generates pure $D\hat{Q}_y = (2\hat{S}_{1x}\hat{S}_{2y} + 2\hat{S}_{2x}\hat{S}_{1y})/2$.⁴⁷ This requires one to add more pulses to \hat{U} in order not to lose the signal.

It is possible to selectively make either C_1 or C_A zero, producing a sum or difference of the terms in $\cos at_x$ and $\cos at_m$. In all cases, the dipolar signal can be acquired using fixed t_m by changing just t_x . This would alleviate (but not remove) issues with relaxation, and nuclear ESEEM should be suppressed to the extent possible. It usually decays as t_m increases. This is what single-resonance PDS sequences have to do in their work. We will show the effects of particular \hat{U} 's when discussing the respective pulse sequences. Briefly, \hat{U} 's in use are $[(\pi/2)_x - t_d - \pi - t_d - (\pi/2)]$; $(\pi/2)_y$; $[(\pi/2)_x - T - (\pi/2)]$; and $[(\pi/4)_y - T - (\pi/4)]$. They make up, respectively, six-, four-, and five-pulse single-resonance experiments that we discuss in the following section.

20.3 DOUBLE-QUANTUM COHERENCE EPR, SIX-PULSE SEQUENCE

20.3.1 Development of DQC EPR

The need to improve sensitivity inspired efforts to develop DQC EPR, which was expected to produce strong dipolar signals, but the initial attempts were not particularly convincing.¹⁹ Renewed effort resolved all issues^{20,21} with the demonstration of strong primary DQC signals, which are well in line with the basic theoretical concepts. Furthermore, the implementation of the method at K_u band at ≈ 17 GHz using an efficient dielectric resonator and intense nanosecond MW pulses^{22,24,62} yielded a very sensitive technique. It is not unusual to obtain a DQC dipolar signal with an SNR in the thousands for a typical spin concentration in the range ~ 100 – 200 μM or as high as several hundreds on lower concentration samples (≤ 50 μM).

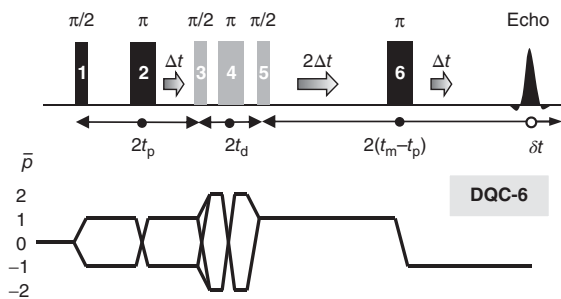


Figure 20.5. The six-pulse DQC sequence is based on RE formed by pulses 1, 2, and 6. The three remaining pulses 3, 4, and 5 constitute a composite propagator \hat{U} , which is a fixed refocusing sequence ($t_d - \pi - t_d$) flanked by $\pi/2$ pulses. The purpose of \hat{U} here is to enable DQ filtering (DQF) by creating DQC from refocused antiphase coherence by $(\pi/2)_x$ pulse 3, refocusing it with the π pulse 4, and then converting it back to antiphase coherence by $\pi/2$ pulse 5, which then evolves to contribute into the detectable echo. This contribution from the spins that have passed through DQC paths is then isolated by performing phase cycling. The pulses are advanced in steps, as shown, as the timing variable is $t_x = t_m - 2t_p$. The recorded signal is symmetric with respect to $t_x = 0$; thus, it usually can be varied just from slightly less than 0 to t_m

20.3.2 Six-pulse DQC EPR Sequence: Basic Principles

The details of the *constant-time* six-pulse DQC sequence depicted in Figure 20.5 are explained elsewhere,^{14,17,22} but a basic description useful for understanding single-resonance methods has been provided in Section 20.2. Here, we limit the discussion to key aspects involved in the function of this important DQC technique before discussing other single-resonance techniques. The pulse sequence in Figure 20.5 is composed of three refocusing sandwiches separated by $\pi/2$ pulses serving to change coherence levels in the desired way. This sequence can be viewed as a constant-time RE sequence of Section 20.2 with two sandwiches centered at π -pulses 2 and 6 separated by the three-pulse propagator, \hat{U} (pulses 3–5), which is used to generate and refocus second-order coherence and then return it back to the $\bar{p} = +1$ pathway where it evolves into detectable coherence at time $2t_m$ after the first pulse labeled 1.

This sequence can also be viewed (as in MQC NMR) as a *preparation – evolution – detection* sequence,⁴⁵ where the first sandwich prepares antiphase coherence, which is converted to DQC, refocused in the evolution

sandwich, and converted back to antiphase coherence evolving in the last sandwich into observable in-phase coherence for detection.

Starting from the equilibrium state $\hat{\sigma}_{12}(0)$, in-phase coherence $\hat{I}_{12} = (\hat{S}_{1y} + \hat{S}_{2y})$ is produced by the first $(\pi/2)_x$ pulse. In the first sandwich, \hat{I}_{12} evolves into $\hat{I}_{12} + \hat{A}_{12}$, with $\hat{I}_{12} = -(\hat{S}_{1y} + \hat{S}_{2y}) \cdot \cos at_p$ and $\hat{A}_{12} = (\hat{S}_{1x}\hat{S}_{2z} + \hat{S}_{2x}\hat{S}_{1z}) \cdot \sin at_p$, and offsets are refocused. The $(\pi/2)_x$ pulse 3 stores the \hat{I}_{12} as $-(\hat{S}_{1z} + \hat{S}_{2z}) \cdot \cos at_p$ and converts \hat{A}_{12} to $DQ_y = -\sin at_p \cdot (\hat{S}_1^- \hat{S}_2^- - \hat{S}_1^+ \hat{S}_2^+)/2i$, which evolves due to the frequency offsets of both spins as $DQ_y(t) = \sin at_p \cdot (\hat{S}_1^- \hat{S}_2^- e^{i(\Delta\omega_1 + \Delta\omega_2)t} - \hat{S}_1^+ \hat{S}_2^+ e^{-i(\Delta\omega_1 + \Delta\omega_2)t})/2i$, with the time t referred to the third pulse. $DQ_y(t)$ is refocused in the $(t_d - \pi - t_d)$ sandwich, and the third $(\pi/2)_x$ pulse 5 converts the resulting $DQ_y(2t_d) = (\hat{S}_1^- \hat{S}_2^- - \hat{S}_1^+ \hat{S}_2^+) \cdot \sin at_p$ back to $\hat{A}_{12} = (\hat{S}_{1x}\hat{S}_{2z} + \hat{S}_{2x}\hat{S}_{1z}) \cdot \sin at_p$ labeled with the phase of the dipolar evolution at $2t_p$. Finally, the last refocusing sandwich evolves \hat{A}_{12} into in-phase $(\hat{S}_{1y} + \hat{S}_{2y}) \cdot \sin(at_m - at_p) \cdot \sin at_p$ and the antiphase $-(\hat{S}_{1x}\hat{S}_{2z} + \hat{S}_{2x}\hat{S}_{1z}) \cdot \cos(at_m - at_p) \cdot \sin at_p$ coherences, of which only the in-phase term is observable.

\hat{I}_{12} at $2t_p$ passes through the $U(\pi/2 - t_d - \pi - t_d - \pi/2)$ propagator, which we will call for convenience a ‘double-quantum filter’ or DQF, for short. The DQF does not actually remove any signal component, rather it ‘labels’ the DQC signal leaving it to the phase cycling to achieve the final filtering. \hat{I}_{12} passes through the DQF as $(\hat{S}_{1z} + \hat{S}_{2z})$ carrying with it the phase $\Phi_{\text{dip}}(2t_p) = \cos at_p$. After the filter, it is again $\hat{I}_{12} = -(\hat{S}_{1y} + \hat{S}_{2y}) \cos at_p$, which evolves into the observable $(\hat{S}_{1y} + \hat{S}_{2y}) \cdot \cos at_p \cdot \cos(at_m - at_p)$. Note that the sum of the two contributions to observable \hat{I}_{12} coherence is $(\hat{S}_{1y} + \hat{S}_{2y}) \cdot \cos at_m$, just as what one expects from the basic RE for pulses 1, 2, and 6 if the DQF is simply viewed as the equivalent of a 2π rotation, which could be a reasonably accurate picture in the absence of coupling and relaxation. It should be emphasized that there is no refocusing of dipolar coupling in the DQC-6 sequence. The refocusing is ‘virtual’ by separating two components constituting the RE into complementary contributions of the refocused type. It is the DQC path enabled by the coupling that makes it possible to separate them by deeply suppressing the unwanted in-phase component by constructing a phase cycle that selects only the pathways passing through DQC order.^{21,24} The basic phase cycle would involve cycling the phases ϕ_k , ($k = 1 \dots 3$) of the pulses 1–3 and the receiver phase ϕ_R in four

steps as $(\phi_1, \phi_2, \phi_3, \phi_R) = \{(x, x, x, y); (y, y, y, -y); (-x, -x, -x, y); (-y, -y, -y, -y)\}$. The last $\pi/2$ pulse as well as all π pulses can be cycled independently to improve the performance, enabling an extended phase cycle sequence up to 256 steps.²¹ This very robust filtering technique provides deep suppression of unwanted coherence pathways irrespective of the arbitrary nature of the pulses or their imperfections. This was also demonstrated at X band³¹ where a standard TE₀₁₂ cavity resonator and 16 ns π pulses were used.

The filtering properties of the DQF have other very important implications. First, we stress that adequate phase cycling^{21,24,63,64} ensures very deep suppression of unwanted pathways. The second key property is that even in the case of strong but finite pulses, π pulses are not able to refocus all the spins, and consequently, they do not invert all the S_z spins in the antiphase coherence terms. This spawns a spurious dipolar trajectory in the evolution, but in this case, the dipolar coupling is refocused in the preparation sandwich, and the respective trajectory does not generate antiphase coherence; consequently, it does not contribute to the DQC pathway selected by the phase cycling and is suppressed. Similarly, the finite refocusing pulse in the detection sandwich after the DQF does not contribute another dipolar trajectory to the amplitude of the detected echo. The same holds for single spins: there is no DQC from them (!) and they can only contribute to the extent that DQC is formed with other spins on surrounding molecules. (This effect becomes insignificant in dilute samples.) This property means that the treatment based on hard pulses describes the performance of this pulse sequence very adequately.

The omitted flip-flop terms in equation (20.2), which exchange dipolar evolutions of coupled spins in an offset-dependent manner, are more difficult to consider in a closed-form analysis, but this has been done under minimal assumptions.²¹ It has been shown that the closed-form expression for the DQC amplitude^{21,65} is adequate for accurate representation of the signal for distances as short as ≈ 1.0 nm given large enough B_1 (>40 G) for such a case of strong coupling. It was also shown that for most practical cases their effects are relatively insignificant. Finally, in a rigorous numerical treatment, one can consider the dipolar coupling during the pulses. What one qualitatively expects from this case is a production of all five coherence pathways including $\bar{p} = \pm 2$ by a finite-length pulse. This case was considered as a central focus in the framework of the generation of ‘forbidden’ DQCs.¹⁹ For the

short intense pulses that we currently employ these effects can safely be neglected for distances greater than ≈ 1.2 nm.

20.3.3 DQC-6: Experimental Examples

We carried out PDS measurements based on the DQC-6 sequence on a variety of spin-labeled systems from synthetic molecules such as biradicals²¹ and peptoids⁶⁶ to proteins.^{31,32,63,67,68} In Figure 20.6, we show examples of DQC measurements conducted on very different systems. In top panel (a), the raw DEER and DQC data obtained on 47 μ M of a 95-kDa soluble LOX-1 enzyme are shown before any background corrections were made. (MTSL-labeled LOX-1 was prepared by B.J. Gaffney and studied in the context of work published in *Biophys. J.*⁶³; This open access work is notable by introducing to PDS a multidimensional scaling approach to perform trilateration for 3D localization by distance geometry of a spin-labeled substrate.) The dipolar modulations are very similar, but the background (see Chapter 19) is considerably smaller in DQC; this subsequently minimizes errors in making background corrections, thus leading to better reconstruction of distances for DQC. This is also helped by the fact that any residual orientational effects are also smaller in DQC due to much less selective pulses (see Section 20.6). In addition, the sensitivity was a factor of nearly 7 higher for the distances in the range 3.5–5.5 nm. The exact reason for the larger factor from that expected of $\approx 2-4$ ²¹ is likely due to a partial suppression of phase relaxation caused by nuclear spin diffusion of the protons,^{24,69-71} yielding a longer phase relaxation time in DQC.

The second example Figure 20.6(b) compares K_u -band DEER and DQC data obtained in measuring the distance between two Cu^{2+} ions.¹³ This case was challenging for both methods used. DEER using strong $B_1 = 30$ G pulses was able only to achieve ≈ 0.05 modulation depth given about 1 kG Cu^{2+} spectral width. It is clear that the large $B_1 = 45$ G we used for DQC could excite only a fraction of the spins. There is still good agreement between the two methods, and again, the sensitivity of DQC was clearly better notwithstanding the fact that π pulses of comparable intensity were used with DEER. In addition, this is an additional demonstration that the DQC technique is not much affected by the fact that there is incomplete spectral excitation. That is, the extent of spectral excitation is not a principal factor for DQC, as

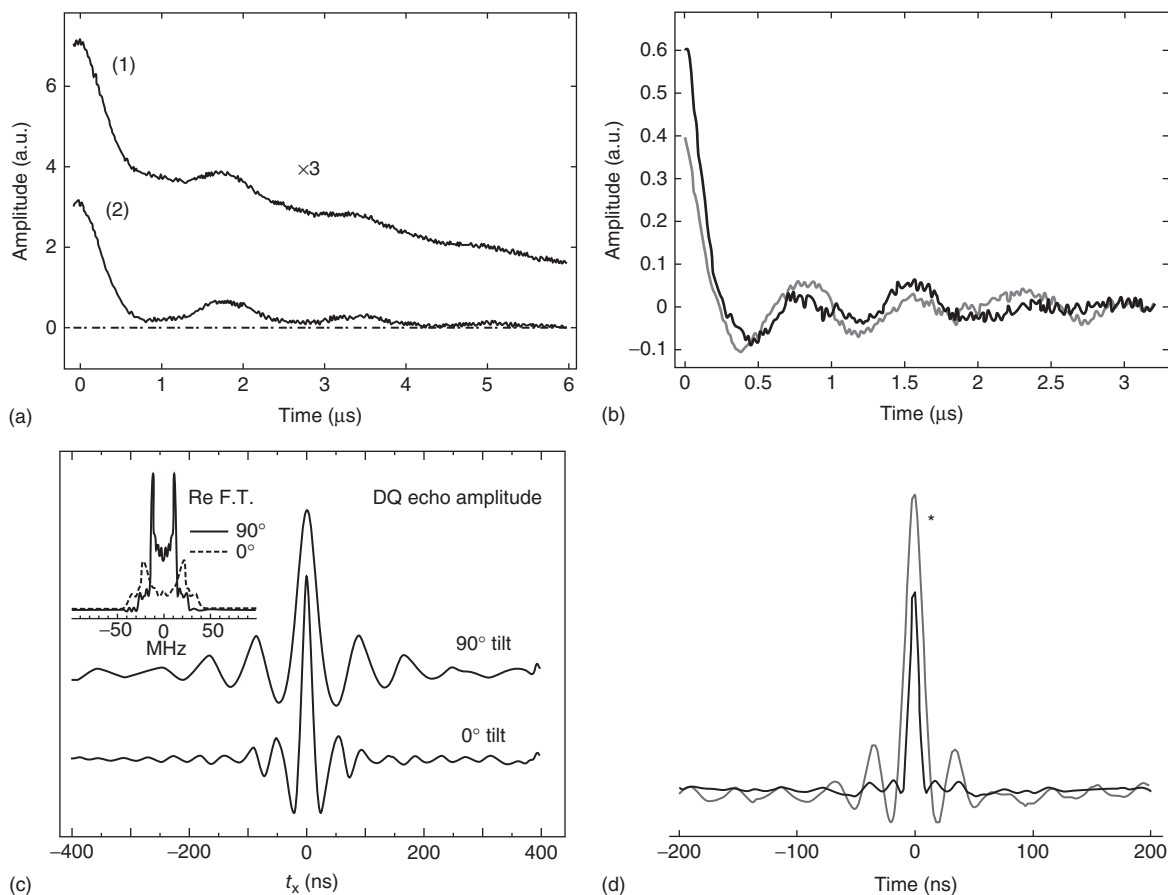


Figure 20.6. (a) Raw 17.3 GHz DQC (2) and DEER (1) signals from soybean lipoxygenase LOX-1 A569R1/A619R1 double mutant in 30% w/v glucose- d_6 /D $_2$ O, 0.1 M tricine buffer, pD 8.4. Protein concentrations were 47 and 160 μ M, respectively. Data averaging time was 5.5 h for (2) and 13.5 h for (1). S/N for equal data averaging time and concentration is a factor of nearly 7 better for DQC. DEER used 16 ns pump pulse, while DQC used 6 ns π -pulses ($B_1 \approx 30$ G). (b) Ku-band DEER (gray) and DQC (black) for Cu $^{2+}$ /Cu $^{2+}$ pair of H48Q human superoxide dismutase SOD-1 fALS mutant. The data were recorded at 20 K at the same (g_y) field position and plotted after making background corrections and scaling to be close in amplitude of dipolar oscillations. DEER was recorded in 13.4 h using 6 ns pump pulse and 140 MHz frequency separation. DQC used 4 ns π -pulses ($B_1 \sim 45$ G) and was recorded in 1.8 h. The dipolar signal is about 6–7 times stronger for DQC, requiring an order of magnitude shorter averaging time than DEER for the same SNR. (Reproduced with permission from Ref. 13. © Elsevier, 2014.) (c) A rigid 1.63 nm nitroxide biradical aligned in nematic LC (phase V) at two director orientations with respect to B_0 recorded at 200 K. (Reproduced with permission from Ref. 21. © Plenum Publishers – Books, 2000.) (d) Ku-band DQC measurements on BTurea and BTXA (starred), which are, respectively, 1.05 and 1.25 nm nitroxide biradicals developed for DNP NMR. (Derived from sample courtesy of R.G. Griffin.) All DQC data (other than (a)) were acquired at 17.3 GHz and 60 K using 2 ns $\pi/2$ and 4 ns π -pulses

the phase cycling provides much greater attenuation of unwanted pathways than other single-resonance methods we consider in the following section, ensuring relatively clean selection of just the desired signal.

One of the first successful DQC measurements included a rigid biradical oriented in a nematic liquid crystal shown in Figure 20.6(c).²¹ The measurements were carried out at -70°C . In the parallel orientation to B_0 , the splitting was ≈ 20 MHz with spectral

components at 32 MHz due to the pseudosecular term also visible.

In Figure 20.6(d), very short distances 1.05 and 1.25 nm were recorded on biradicals developed for DNP^{22,72} without encountering any significant problem. The first distance is about the shortest DQC can measure as the dipolar coupling constant $\omega_{dd}/2\pi$ is 45 MHz (≈ 16 G), which according to our numerical simulations⁶⁵ is close to maximum for a B_1 of 45 G. For greater dipolar coupling, its presence during the pulse should be considered and $J(r_{12})$ is likely to become large.

All the abovementioned measurements used a 64-step phase cycle for DQ filtering. This phase cycle was derived from the full 256-step phase cycle described in²¹ as follows: the first 32 lines in the phase cycle table are copied to make lines 33–64. In this table for the 32 added lines, the phase of the sixth pulse is y and the receiver phases inverted. The CYCLOPS steps used for constructing the 128- and 256-step phase tables were omitted. Nuclear ESEEM from protons was suppressed by summing four data sets with t_m incremented for the subsequent set by half a period (19 ns) of the ESEEM. This describes one of the standard ESEEM suppression routines we developed to record DQC (and DEER) data¹⁴; other approaches used with low-resolution timing are also known.⁶³

20.4 FOUR- AND FIVE-PULSE ‘SINGLE-QUANTUM COHERENCE’ PDS SEQUENCES

20.4.1 The Four-pulse SIFTER Experiment

The adoption of key NMR pulse methods added to PDS a group of four- and five-pulse constant-time single-resonance experiments.^{8,21,23} Similar to DQC, they benefit from applying strong (almost) nonselective pulses, potentially covering nearly the entire spectral width for a nitroxide. The methods are based on simultaneous manipulation with the coherences of the two spins by switching the course of evolution of dipolar coupling in the RE sequence (see Section 20.2). The specifics are in how the refocused signal is modified in each case.

We now discuss single-resonance pulse sequences that can benefit from strong pulses by first assuming ideal infinite pulses to simplify the initial discussion. In Figure 20.4, we show an RE, which is at the

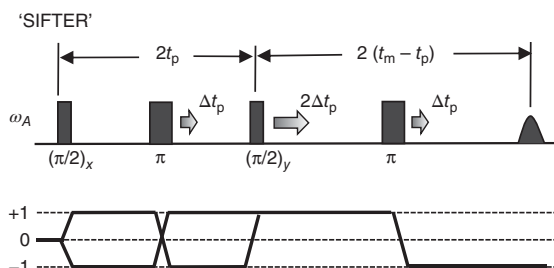


Figure 20.7. The four-pulse SIFTER SQC sequence. The CPT chart shows that the sequence is essentially an RE discussed in Section 20.2. The refocusing propagator U in this case is just a $(\pi/2)_y$ pulse. It exchanges the antiphase coherences of the two spins, thus making coherence transfer. (The transfer also includes electron–nuclear but not nuclear coherences.) The sequence is ‘constant time’ with the position of the echo at $2t_m$ being constant. The pulses advance in steps shown, starting, e.g., at $t_p = 0$. The relevant time variable $t_x = t_p - (t_m - t_p) = 2t_p - t_m$ spans the range of $[-t_m, t_m]$

basis of DQC-6 and several other single-resonance techniques including the four-pulse single-frequency technique for refocusing (SIFTER) pulse sequence depicted in Figure 20.7 and discussed in this section. The pulse sequence described here was implemented in EPR in 2000²³ and was named SIFTER. According to Figure 20.4(a) and the subsequent discussion, it is not possible with nonselective π -pulses to refocus simultaneously frequency offsets and dipolar coupling. We have shown there and reiterate here the argument that a single nonselective $(\pi/2)_y$ pulse can, however, completely refocus the coupling.

The sequence based on RE has two refocusing $t_p - \pi - t_p$, and $(t_m - t_p) - \pi - (t_m - t_p)$, sandwiches. The evolution after the first sandwich produces

$$\hat{\sigma}_{12}(2t_p) = -(\hat{S}_{1y} + \hat{S}_{2y}) \cos at_p + (2\hat{S}_{1x}\hat{S}_{2z} + 2\hat{S}_{2x}\hat{S}_{1z}) \sin at_p \quad (20.21)$$

In the absence of the $(\pi/2)_y$ pulse, this would then evolve, as we showed in Section 20.2.7 to produce $\hat{\sigma}_{12}(2t_m) = (\hat{S}_{1y} + \hat{S}_{2y}) \cos at_m$ and is not very useful as the dipolar coupling is in the t_m variable, but this $(\pi/2)_y$ pulse changes the sign of the antiphase term by effecting CT according to $2\hat{S}_{1x}\hat{S}_{2z} \leftrightarrow -2\hat{S}_{2x}\hat{S}_{1z}$ so that the evolution through the second sandwich now gives $\hat{\sigma}_{12}(2t_m) = (\hat{S}_{1y} + \hat{S}_{2y}) \cos at_x$, permitting one to record the evolution as a function of the new variable $t_x = 2t_p - t_m$. It also permits one to record the full

echo, 100% modulated with the dipolar oscillations, which is a very attractive property of this pulse sequence. Unlike DQC-6, there is no constant term in $(\hat{S}_{1y} + \hat{S}_{2y})\cos at_m$.

20.4.2 Effects of Finite Pulses in SIFTER

We have discussed SIFTER in the hard-pulse limit using POs to describe the spin dynamics. Performance with real finite pulses complicates the case to some extent. We will now look into the main implications of finite pulses with SIFTER. SIFTER does not have a mechanism for filtering (see Section 20.3.3). Therefore, with real finite pulses, all possible dipolar trajectories (see Section 20.2) will be produced and detected. Specifically, what happens during each refocusing sandwich in the case of finite pulses can be described as follows. We assume that the finite π -pulse can flip a fraction p of spins while the fraction $q = 1 - p$ remains unaffected (for a subensemble of single spins $q = 1$). Otherwise, the pulses are taken as ideal. The evolution proceeds as

$$\begin{aligned} \hat{S}_{1y} &\xrightarrow{t_1 - \pi - t_1} -q\hat{S}_{1y} + p(\hat{S}_{1y}\cos at_1 + 2\hat{S}_{1x}\hat{S}_{2z}\sin at_1) \\ &\xrightarrow{(\pi/2)_y} -q\hat{S}_{1y} + p(\hat{S}_{1y}\cos at_1 - 2\hat{S}_{1x}\hat{S}_{2z}\sin at_1) \\ &\xrightarrow{t_2 - \pi - t_2} \hat{S}_{1y}[(q + p\cos at_1)(q + p\cos at_2) \\ &\quad + p^2(-\sin at_2)\sin at_1] + 2\hat{S}_{1x}\hat{S}_{2z}(\dots) \end{aligned} \quad (20.22)$$

The $(\pi/2)_y$ pulse changes the sign of the antiphase term as $(\hat{S}_{2x}\hat{S}_{1z} + \hat{S}_{1x}\hat{S}_{2z}) \rightarrow -(\hat{S}_{1x}\hat{S}_{2z} + \hat{S}_{2x}\hat{S}_{1z})$. The evolution for the second spin is obtained by swapping subscripts 1 and 2. One thus detects

$$\begin{aligned} (\hat{S}_{1y} + \hat{S}_{2y})\{q^2 + pq\cos[a(t_m - t_x)/2] \\ + pq\cos[a(t_m + t_x)/2] + p^2\cos at_x\} \end{aligned} \quad (20.23)$$

The last term in $\cos at_x$ in equation (20.23) has its maximum at $t_x = 0$ in the center of evolution interval $[-t_m, t_m]$ as we found from this sequence with hard pulses. The first term is a constant background, whereas the next two terms are dipolar signals oscillating at half the dipolar frequency, and they start at the opposite ends of the full evolution interval in t_x . For the pulse sequence to be useful, the condition $p \gg q$ for spins contributing to the signal should be met, so only the last term is significant. This would be difficult to accomplish even for nitroxides but is more feasible for much narrower spectra such as trityl

or some organic radicals (e.g., tyrosyl or flavin radical cofactors). Single spins, if present, will add to the background term in q^2 . The only way to deal with these issues is to achieve the conditions to ensure small q for spins contributing to the signal using very intense pulses or shaped pulses designed to minimize the product term $p(\Delta\omega)q(\Delta\omega)$ by achieving uniform profile of $q(\Delta\omega) \approx 0$ for flipped spins⁷³ (see Chapter 21).

The situation is markedly different in DQC-6. As discussed in Section 20.3.3, phase cycling selects only those coherences that have passed through the DQC channel. Consequently, single spins do not contribute to this signal. For finite pulses, as we discussed, this is also true for that fraction of coupled spins where only one offset-refocused spin was effected by the first π pulse; consequently, they do not contribute to any DQ-filtered pathway and are suppressed, so only the p^2 term is detected. Thus, with finite pulses, the performance of DQC-6 is not beset with the problems one has to address with SIFTER.

20.4.3 An Example of SIFTER and DQC-6 with Strong- B_1 Pulses

We demonstrate the abovementioned discussion with (not previously published) experimental SIFTER and DQC-6 data obtained using a typical case of a soluble MTSL double-labeled protein T4-lysozyme (T4L), for which extensive DEER^{74,75} and DQC^{14,22,31} data have been published. The measurements were carried out at K_u band (17.3 GHz).

We show in Figure 20.8 the data from SIFTER and DQC-6 applied to T4L double labeled at sites 80 and 128 and prepared in both H_2O and D_2O . Intense B_1 pulses of 45 G were used to produce π pulses of 4 ns in all four cases. Yet, even such intense pulses are still insufficient to attain complete inversion of the ^{14}N nitroxide spectrum; therefore, significant background appearing as double frequency modulations is still present in SIFTER, particularly visible for H_2O , because the spin labeling efficiency was ≈ 0.8 in this case. Single spins do not add any type of dipolar signal, except for intermolecular effects. In the case of protons, the background is strongly decaying with an approximately Gaussian profile, the decay being mostly due to nuclear spin diffusion^{22,70,76,77} but also to ID. The decays are generally slower than for a two-pulse PE, as SIFTER uses two refocusing pulses that partially suppress nuclear spin diffusion, making the phase memory time T_m about a factor of $2^{1/2}$ longer than for the

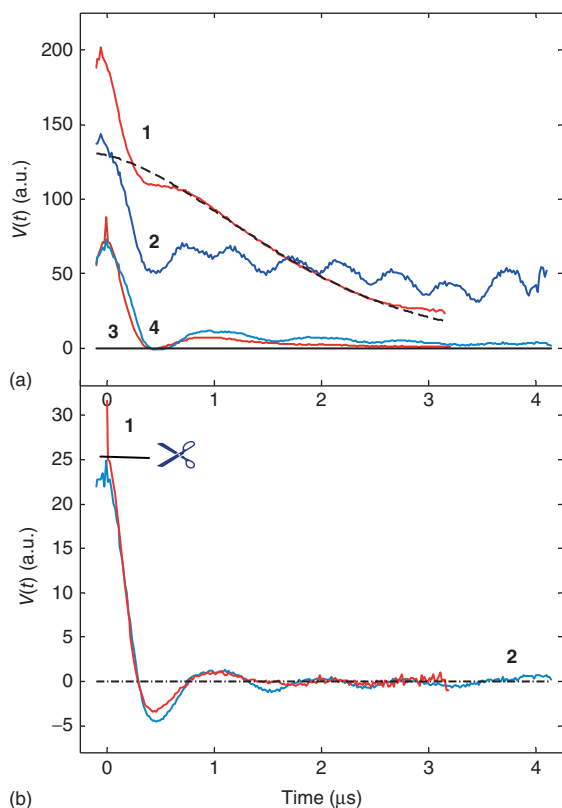


Figure 20.8. (a) 17.3 GHz SIFTER (1, 2) and DQC (3, 4) data taken on a 15- μl sample of T4 Lysozyme, double labeled with MTSL at positions 80 and 128. Samples were prepared in either H_2O or D_2O working buffers. Protein concentration was 48 μM in H_2O buffer (1, 3) and 42 μM for D_2O (2, 4). Spin-labeling efficiency was 0.8 for the H_2O sample and ≈ 1 in case of D_2O , as estimated using the DEER modulation depth. (The data for H_2O and D_2O are not plotted to the same scale.) The DQC data were scaled up by the factor of ≈ 2.5 to match the intensity of dipolar oscillation in SIFTER. The dashed curve for 1 is then fit to the baseline, whose temporal profile is dominated by nuclear spin diffusion ($\sim \exp[-(2t/T_{\text{nsd}})^\kappa]$, $\kappa \approx 2$, $T_{\text{nsd}} \approx 4 \mu\text{s}$ for H_2O solutions) and ID (see Section 20.7). This was done by subtracting (3) from (1) and then fitting to a third-order polynomial the logarithm of the remainder without using the latter 1 μs of the record distorted by spurious contributions. All pulse sequences used $\pi/2$ pulses of 2 ns and π pulses of 4 ns, sample temperature was 60 K. A 64-step phase cycle was used for DQC, as well as for SIFTER. Data averaging times were 1 h for 1 and 3 and 4.6 h for 2 and 4. (b) The DQC data sets shown in (a) are plotted after making corrections for the small background present in the raw data (3 and 4)

PE.^{22,69} In cases of stretched exponential decay²⁴ as is the case here, the relaxation envelope is present in the data because the time intervals $t_1 = t_p$ and $t_2 = t_m - t_p$ are variable.^{22,69} There are no such problems in DEER as the detection pulse sequence is fixed.

DQC-6 exhibits a very small baseline, so that even deep ESEEM by deuterium nuclei does not appear as a significant problem. The data for H_2O and D_2O are similar, with somewhat deeper dipolar oscillations in D_2O . Note that for H_2O the DQC data are also modified by relaxation caused by nuclear spin diffusion,³¹ although the contribution to the decay due to ID is expected to be less than in SIFTER (see Section 20.7). The decay could result in a small broadening of the reconstructed distance distributions for distances < 5 nm and can be partly corrected,³¹ if so desired. As the background is very small, it is much easier to correct for it than in DEER and introduces smaller errors. We do find that Tikhonov regularization^{22,78} can often be applied directly to DQC data to reconstruct distances without any baseline correction, leading to low-intensity broad humps at long distances, but with little if any effect on the main distance peaks at moderate and short distances.

20.4.4 Five-pulse SQC Sequences, Jeener–Broekaert Sequence

There are two five-pulse constant-time sequences (Figure 20.9) that operate with respect to the pulse position in the same manner as six-pulse DQC or SIFTER in that they have similar time variables, which in the case of DQC-6 are the sum (t_m) and difference (t_x) of two interpulse intervals. The two pulse sandwiches in RE are connected by a pulse propagator U , which performs the desired transfer of \hat{I}_{12} , \hat{A}_{12} from the first (preparation) to the second (detection) sandwich to accomplish the refocusing of dipolar coupling evolution according to the discussion in Section 20.2.7. All these propagators start from a pulse, for which we use $(\pi/2)_x$ in DQC and $(\pi/2)_y$ in SIFTER. But now the pulse propagator U is much different, as it relies on phase relaxation to remove unwanted coherences. The sequences store selected coherences as polarizations for long enough time for unwanted transverse coherences to decay by phase relaxation. The storage period also allows one to manipulate other coupled spins, if such are present.³⁸ In general form, we expect the sequence to be described

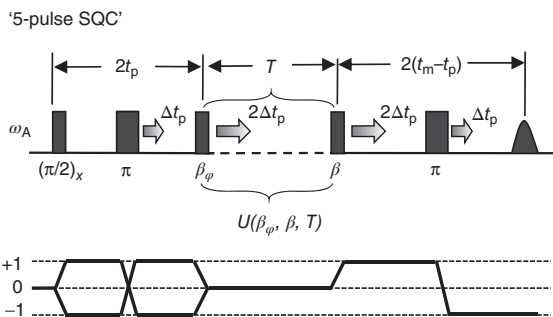


Figure 20.9. Five-pulse PDS ‘single-quantum coherence’ (SQC) sequences designed to store dipolar evolution for manipulation with coherences. The first $t_p - \pi - t_p$ sandwich prepares in-phase and antiphase coherences labeled by $\cos at_p$ and $\sin at_p$, respectively. When the β_φ pulse is $(\pi/2)_x$, it stores these coherences as polarizations, i.e., in longitudinal magnetizations and dipolar order with β , φ , B_1 (and spectral shape) determining their ratio. A hard $(\pi/2)_x$ pulse stores in-phase coherence as z -magnetization, whereas hard $(\pi/4)_y$ stores antiphase coherence in dipolar order $2\hat{S}_{1z}\hat{S}_{2z}$. In the latter case, the sequence functions as the Jeener–Broekaert sequence. After a storage period, $T \gg T_m$ all other coherences decay owing to phase relaxation with memory time T_m . A subsequent β -pulse ($\beta = \pi/2$, or $\pi/4$ for dipolar order) reads stored coherences back into SQCs, which then evolve into a detectable echo

by an arbitrary pulse sequence: $\alpha - t_p - \beta_1 - t_p - \beta - T - \beta - (t_m - t_p) - \beta_1 - (t_m - t_p)$ -echo,²¹ where we do not define the pulse phases but nominally let $\alpha = \pi/2$ and $\beta_1 = \pi$. Then, the first $\hat{S}_{1y} + \hat{S}_{2y}$ evolves as given by equation (20.21); the coherences $(\hat{S}_{1y} + \hat{S}_{2y})$ and $(\hat{S}_{1x}\hat{S}_{2z} + \hat{S}_{2x}\hat{S}_{1z})$ are transformed by the β -pulse and remain stored during the time $T \gg T_m$ as

$$\begin{aligned} & \hat{S}_{1z} + \hat{S}_{2z}, \quad 2\hat{S}_{1z}\hat{S}_{2z}, \quad + (\text{transverse terms}) \\ & \xrightarrow{T} \hat{S}_{1z} + \hat{S}_{2z}, \quad 2\hat{S}_{1z}\hat{S}_{2z} \end{aligned} \quad (20.24)$$

Then, $(\hat{S}_{1y} + \hat{S}_{2y})$ and $-2\hat{S}_{1x}\hat{S}_{2z} - 2\hat{S}_{2x}\hat{S}_{1z}$ are produced by the β -pulse and evolve to the final $\hat{S}_{1y} + \hat{S}_{2y}$ labeled with the respective dipolar evolution-dependent factors.²¹

If the DQC-6 refocusing pulse is omitted and a long pulse interval $2t_d = T$ is used, all transverse coherences will decay by phase relaxation except for the in-phase coherence that passes through the filter as S_z irrespectively of refocusing. Thus, in such a five-pulse single-quantum coherence sequence (in-phase SQC-5), the $(\pi/2)_x$ pulse stores coherence S_y as S_z , and the subsequent $\pi/2$ pulse generates the

coherences contributing to the echo. These coherences are not always labeled by the dipolar interaction, e.g., for a single spin or if the π pulse in the preparation sandwich refocuses dipolar coupling. Therefore, significant background may be present. This background can be modulated by nuclear ESEEM, which is particularly detrimental in the case of deuterons (Figure 20.10a) or nitrogen ligands.^{7,13,44,79}

As we showed (see Section 20.2.7) and recapitulate here, two refocusing propagators produce:

$$\begin{aligned} & \hat{S}_{1y} + \hat{S}_{2y} \xrightarrow{t_1 - \pi - t_1} \xrightarrow{t_2 - \pi - t_2} (\hat{S}_{1y} + \hat{S}_{2y}) \\ & \times (\cos at_1 \cos at_2 - \sin at_1 \sin at_2) \end{aligned} \quad (20.25)$$

which is proportional to $\cos at_m$. This is the same result as for RE. The similar echo signal is detected in DQC-6 before the second term in equation (20.25) is extracted by filtering out the rest using appropriate phase cycling to give $-\sin at_1 \sin at_1 = (\cos at_m - \cos at_x)/2$, which presents the refocused dipolar signal that we need for recording its dependence on a time variable, e.g., $t_x = t_1 - t_2$ in a constant-time PDS pulse sequence. If any of the two terms in equation (20.25) are removed ‘physically’, e.g., by relaxation, the outcome is similar, in that a large fraction of spin pairs may have the coupling refocused. As the terms in equation (20.25) depend on in-phase and antiphase coherences at time $2t_1$, modifying them separately solves the problem. This was implemented in SIFTER by complete refocusing of dipolar coupling accomplished by inverting the sign of just the antiphase coherence term. As in-phase and antiphase coherences refocus on different axes in the rotating frame, they can be stored selectively as polarization and then converted back to transverse coherence that will evolve into one of the terms in equation (20.25).

A better use of the five-pulse sequence was reported as a PDS pulse sequence²³ based on the Jeener–Broekaert (JB) technique^{42,80} for creating two-spin dipolar order, $2\hat{S}_{1z}\hat{S}_{2z}$. In this technique, a $(\pi/4)_y$ pulse is employed for β_φ to convert the antiphase coherence $(\hat{S}_{1x}\hat{S}_{2z} + \hat{S}_{2x}\hat{S}_{1z})$ to $2\hat{S}_{1z}\hat{S}_{2z}$, which immediately follows from

$$\begin{aligned} & 2(\hat{S}_{1x}\hat{S}_{2z} + \hat{S}_{2x}\hat{S}_{1z}) \xrightarrow{(\pi/4)_y} 4(\hat{S}_{1x} + \hat{S}_{1z})2^{-1/2} \\ & \times (\hat{S}_{2x} + \hat{S}_{2z})2^{-1/2} \\ & = 2\hat{S}_{1z}\hat{S}_{2z} + \text{transverse terms} \end{aligned} \quad (20.26)$$

The transverse terms (ZQ , DQ , and antiphase SQ) vanish after a sufficient storage time $T \gg T_m$ so that

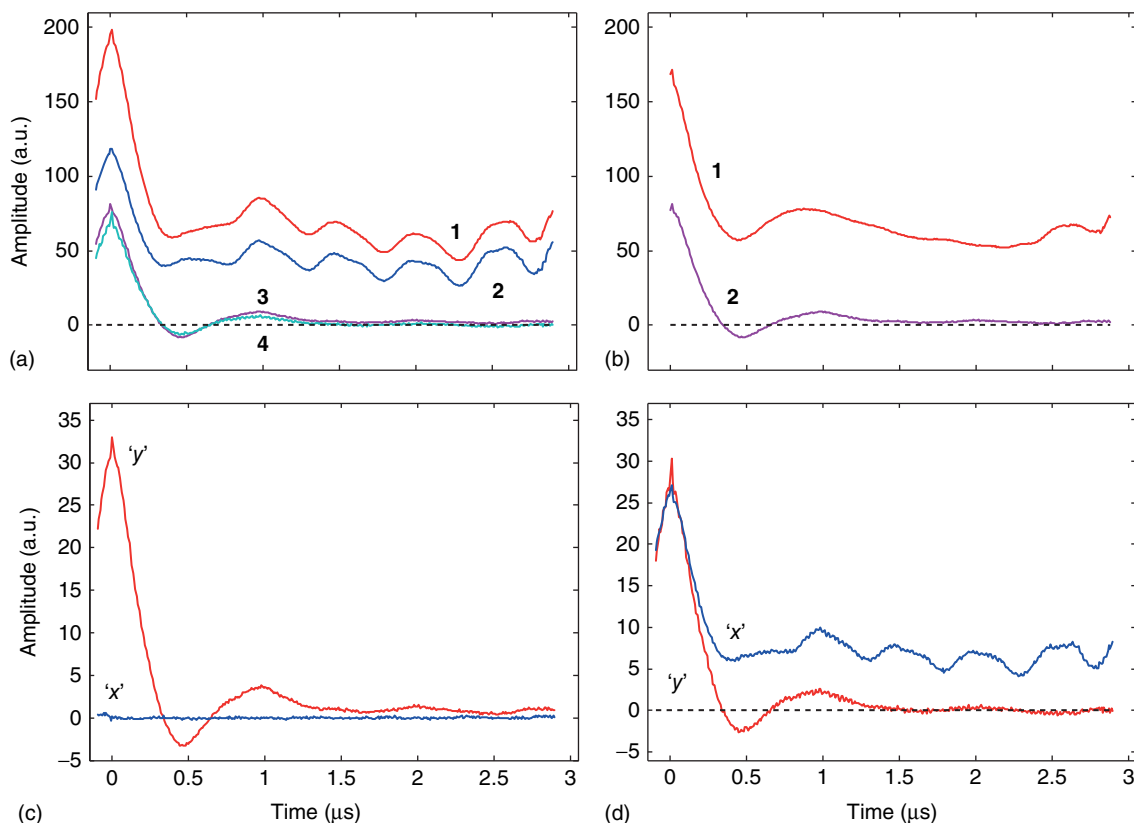


Figure 20.10. The six-pulse DQC and three SQC PDS sequences are compared. For the purpose of this article, comparative measurements were carried out. All data were taken on a 15- μl sample of 38 μM 80/135 MTSL-labeled mutant of T4-Lysozyme in 30% (w/v) glycerol- d_8 /D₂O based buffer at 17.3 GHz and 60 K. (a) Shown are the data for SIFTER (1); five-pulse in-phase SQC (2); DQC-6 (3); and JB (4) sequences. The data were recorded in succession using the same sample and fixed receiver gain. In all cases, the $\pi/2$ and π pulses were 2 and 4 ns; for $\pi/4$ pulses in the JB sequence, the pulse duration was adjusted to about 1.5 ns to maximize the signal (b) DQC (2) is compared to SIFTER (1) with ²H ESEEM filtered out using 2 and ≈ 4 MHz bandpass filters. The DQC signal was multiplied by 2.5. SIFTER exhibits a strong unwanted dipolar pathway visible at the end of the record, as the pulses are not yet ideal hard pulses. (c) Raw DQC data with y and x components shown. (d) JB data shows both y and x components. Plots (c) and (d) have a common vertical scale

only the dipolar order term $2\hat{S}_{1z}\hat{S}_{2z}$ labeled with $\sin at_p$ remains. Then another $(\pi/4)_y$ converts half of dipolar order to first-order antiphase coherence according to

$$\begin{aligned} 2\hat{S}_{1z}\hat{S}_{2z} &\xrightarrow{(\pi/4)_y} 2(\hat{S}_{1z} - \hat{S}_{1x})2^{-1/2} \times (\hat{S}_{2z} - \hat{S}_{2x})2^{-1/2} \\ &= -(2\hat{S}_{1x}\hat{S}_{2z} + 2\hat{S}_{2x}\hat{S}_{1z})/2 + \text{other orders} \end{aligned} \quad (20.27)$$

The antiphase term labeled with $\sin at_p$ evolves into an observable signal, while the other orders (ZQ, DQ, dipolar order) do not lead to any detectable signal. The fact that antiphase coherence gets refocused by

having its sign changed after a storage time T is of little interest, as the refocused in-phase coherence $-(\hat{S}_{1y} + \hat{S}_{2y})$ produced by the preparation sandwich simply does not survive the storage time, and in this case of ideal pulses, the lone antiphase term evolves into

$$\begin{aligned} \hat{S}_{y,\text{detect}} &= (1/2)(\hat{S}_{1y} + \hat{S}_{2y}) \sin at_p \sin(at_m - at_p) \\ &= -(\hat{S}_{1y} + \hat{S}_{2y})(\cos at_x - \cos at_m)/4 \end{aligned} \quad (20.28)$$

This is half the amplitude of the DQC-6. There is no in-phase component in S_x 's if the pulses are nonselective. (The detected echo would be an out-of-phase

echo (i.e., on the x -axis) if $(\pi/4)_x$ were used to read out dipolar order.) As in DQC-6, the dipolar coupling is only partly refocused. The JB sequence thus relies on ‘physical’ filtering out (by relaxation) of the first term in equation (20.25).

20.4.5 Comparison of DQC and SQC Single-resonance PDS Sequences

The literature data,²³ obtained at X-band on rigid biradicals using relatively soft pulses, demonstrated the feasibility of SQC methods but yielded obscure signals unlike the results on biological samples by DQC-6 conducted under similar conditions.³¹ To compare all these methods on biological samples under better experimental conditions that we now routinely employ with DQC, we conducted several measurements on a spin-labeled protein using all four single-resonance methods described earlier. The results are compared in Figure 20.10(a), where the raw data for three SQC PDS sequences and DQC are shown. All experiments were conducted on the same sample and at an otherwise identical instrument setting. The SIFTER pulse sequence and the in-phase SQC-5 in Figure 20.10(a) and (d) are very similar in their outcome, except the SIFTER signal is about a factor of 2 stronger, as expected. We used deuterated solvent, making relaxation slow on the timescale used. Both signals have significant background, which is deeply modulated by deuterons. Filtering ESEEM out numerically (Figure 20.10b) reveals for the SIFTER at the end of the record a large spurious dipolar signal oscillating with half the dipolar frequency (equation (20.23)). However, the DQC-6 signal is clean, has low background, and shows very little presence, if at all, of nuclear ESEEM.

In Figure 20.10(c) and (d), the x and y components of the DQC-6 and JB pulse sequences are shown. Note that in the JB sequence the echo is formed on the axis orthogonal to that for in-phase SQC-5. That is, a so-called out-of-phase echo, similar to that observed in light-induced spin-correlated radical pairs (SCRPs), is discussed later in text.

This property helps to separate the signal in the JB sequence from those that involve in-phase coherence stored as \hat{S}_z . It should be noted that, expectedly, there is a contribution of the SQC-5 type in the x projection of the signal in JB, as it is difficult to adjust short and intense but still finite pulses to completely

avoid having an admixture of the two signals. However, these signals should be significantly out-of-phase as the longitudinal terms $\hat{S}_{1z} + \hat{S}_{2z}$ and $2\hat{S}_{1z}\hat{S}_{2z}$ after, e.g., the $(\pi/4)_y$ pulse will evolve to produce echoes on the x and y axes, respectively. A careful look at the JB signal recorded using different pulses shows that there is indeed an admixture of signals on each axis, so some additional empirical signal phasing and referencing is needed to ensure clean data. But then the relevant data for DQC and JB are close to each other. With ideal pulses, there should be a factor of 2 smaller signal for JB sequence, but DQC refocusing at the two spin frequencies with a third π -pulse reduces this amplitude by a factor of $\approx 2/3$, as the spectral excitation for N π -pulses can be shown to depend on N as $N^{-1/2}$ and leads to a factor of $(2/3)^{1/2}$ for each spin and $2/3$ overall.²¹

The filtering properties of these two pulse sequences (DQC-6 and JB) reject the signal from single spins, so ideally there should be no background due to their presence. However, antiphase coherences are formed in the bath of single spins, so there will be some background increasing with concentration and evolution time. SIFTER and SQC-5 do allow the single-spin signal to go straight to the output, but its time dependence does not carry any dipolar modulation; however, it does contain relaxation, ESEEM, and intermolecular decay effects. Thus, this means that there is uncertainty with the nature of the background. Such uncertainty to a varying extent is inherent in all PDS methods. For DQC and JB, the background is minimal, so these issues are less important.

In both DQC and JB sequences, complete spin mixing occurs during DQ or dipolar order evolution periods. These orders are symmetric with respect to spin permutations; therefore, half of the spins will undergo CT as in SIFTER, i.e., the evolution starts on one spin and ends on its partner, whereas the other half remains unchanged. This should have consequences for orientational correlation experiments described in Section 20.6. Therefore, there is a mixture of signals that could depend differently on orientational correlations between the two spins. In the ideal case of four-pulse SIFTER, there is no such mixture, as only refocusing of dipolar coupling takes place, and the principal signal is of the CT type. In the real case, there are unwanted pathways, and the background, all of which do not have the CT property, and they need to be suppressed in order not to obscure the main signal.

At present, with rectangular pulses, DQC-6 and JB sequences present a better choice for distance measurements. In our limited experience with SQC sequences, we find it is more complex to implement JB filtering compared to DQ filtering. The latter is very forgiving for pulse and phase mistuning. A long storage time T is needed in the JB sequence creating some extra complications with the pulse amplifier, more so when it is a TWTA.

20.4.6 SIFTER and DQC on Trityl Biradical

Even though SIFTER yields the strongest dipolar signals, there are currently only a few examples of its applications in the literature. This is not entirely unexpected but is due to the extent of unwanted effects that are difficult to avoid in a multipulse EPR pulse sequence with finite pulses. This greatly complicates what could work perfectly otherwise. This has also been our experience with this group of methods. Over the course of 15 years, we have conducted a substantial number of DQC experiments, and in many of these cases, SIFTER has also been attempted, but even with the largest B_1 's available to us (45 G), the outcome was as a rule too convoluted, with an admixture of unwanted dipolar signals, making the task of removal of unwanted signals and background correction an uncertain procedure leading to large residual errors. The background, as we see in Figures 20.8 and 20.10, in addition to relaxation decay, could be modulated with a strong nuclear ESEEM, for which a higher working frequency than K_u or even K_a band would be needed to make them smaller.

While proton ESEEM is easily suppressed by four-point averaging for protons,^{21,31} often deep low-frequency ESEEM of the background by deuterium or nitrogen nuclei is very objectionable, easily overwhelming the dipolar signal, especially when spin labeling efficiency is not high enough, as is frequently the case. This was also true for in-phase SQC-5, which also requires (nearly) ideal pulses. Nevertheless, systems with narrow EPR spectra can be more amenable to SIFTER and SQC-5. A good target is the trityl radical, which could be studied even at ambient temperature in liquids.⁶⁸ One does not necessarily expect efficient spin labeling with trityl, so the single-label background could substantially hamper these two methods. Both, JB and DQC-6, however, have good filtering properties. DQC-6 yields slightly

higher signal and (at least in our experience) is easier to perform. In part, this is caused by the need to set up three types of pulses, and the second issue is with the TWTA, which has to stay in transmission mode longer by $\approx T$, so that one has to break it into a sequence of shorter transmissions, leading to signal artifacts. DQC indeed was very successful for trityl-labeled immobilized T4L⁶⁸ and RNA⁸¹ in solutions at ambient temperatures. None of these single-resonance sequences (DQC included) is expected to work in the case of high-spin Gd^{3+} due to its very large pseudosecular term and a potential to exhibit multiple higher coherences within each spin. (All our attempts to detect at 17 GHz and 10 K a DQC signal on the narrow central transition of $Gd^{3+}/DOTA$ in 60 μM sample of doubly labeled T4L 8C/128C mutant thus proved unsuccessful. The DEER signal, however, was readily recorded yielding an SNR of about 30% of that for these sites labeled with MTSL, being recorded at 60 K. The lower SNR for Gd^{3+} compared to MTSL may be due to the insufficiently high working frequency of 17 GHz, as Gd^{3+} DEER becomes efficient at frequencies at Q-band (33–50 GHz) and above.)

SIFTER was successfully conducted on a trityl biradical in frozen solution with the results shown in Figure 20.11 where it is compared to those of DQC-6.⁸² The time-domain data from both techniques are very similar but not identical, as modulation is more pronounced in SIFTER. The distance distributions reconstructed with DeerAnalysis 2013⁸³ are also different. The supplementary information for this work indicated large enough backgrounds so that even for this narrow spectrum there is still greater potential for uncertainty in extracting the dipolar signal in SIFTER compared to DQC, thus showing SIFTER requires still harder pulses than the 22 ns π -pulses used as well as tougher requirements for spin labeling.

20.4.7 New Approaches Based on Uniform Spectral Excitation by Adiabatic Pulses

As we have shown, even for sufficiently intense pulses, there still is a problem with the outcome of SQC (as distinct from DQC) PDS experiments. Even more intense pulses may be desirable, but this would require smaller resonators than we currently employ with some loss of sensitivity possible. It is also worth mentioning that relaxation, nuclear ESEEM, and flip-flop

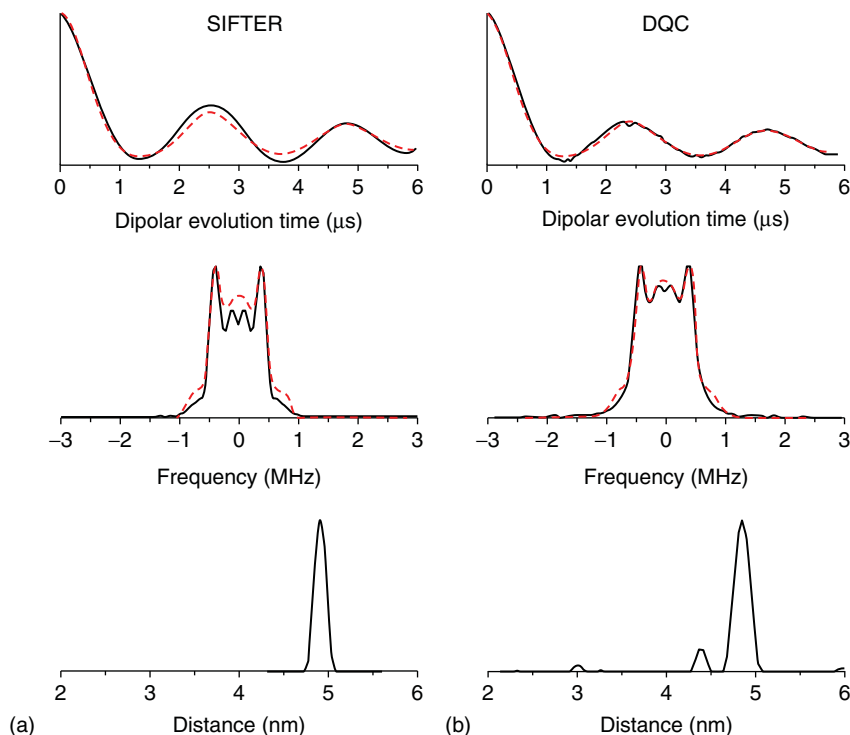


Figure 20.11. SIFTER (a) and DQC-6 (b) experiments performed on a trityl biradical at Q-band ≈ 34 GHz and 50 K. Widths of π -pulses were 22 ns. (Top) Shown here are background-corrected data traces (solid) and time traces (dashed) generated from the distance distribution as reconstructed using Tikhonov regularization included with DeerAnalysis software. (Middle) Fourier transforms of the background corrected SIFTER and DQC time traces plotted as normalized to the maxima of the Pake patterns. The transforms of the experimental time traces (solid) and the fitted traces (dashed) are shown. (Bottom) Distance distributions reconstructed from the data (top row) using Tikhonov regularization in DeerAnalysis. (Reproduced with permission from Ref. 82. © Royal Society of Chemistry, 2015)

terms in the secular dipolar Hamiltonian contribute a considerably more severe problem in single-resonance techniques compared to double resonance, where they can be avoided or minimized by having the detection pulse sequence fixed and pump pulses applied at large enough spectral separation from the detection sequence. On the other hand, these problems may in principle be overcome using adiabatic pulses that can provide more uniform spectral excitation to help to bring the performance closer to that expected from ideal hard pulses (see Chapter 21). Various types of shaped pulses present a possible approach permitting more uniform excitation, refocusing, and population inversion with spectral coverage that is wider than the typical nitroxide spectral width, or alternatively the shaped pulses could have a sufficiently rectangular

excitation profile over a limited spectral extent to reduce the contribution of unwanted dipolar trajectories. Single spins would then remain the only source of the background but, unlike in DEER, may be more severely affected by nuclear ESEEM; thus, a higher working frequency would be of help with alleviating this issue. Such approaches, indeed, were recently tested with SIFTER.^{73,84} In one approach tested on a biradical (Figure 20.12a),⁷³ the back-to-back $(\pi/2)_x - t_1 - \pi - t_1$ and $(\pi/2)_y - t_2 - \pi - t_2$ adiabatic PE sequences with 2:1 pulse width (or more precisely, inverse frequency sweep rates) ratio were employed for echo offset refocusing without time dispersion.⁸⁵ Using such adiabatic-pulse-based SIFTER at X-band with a 1-kW power source, a background of only 5% (Figure 20.12b) survived, but at Q band, with only 10

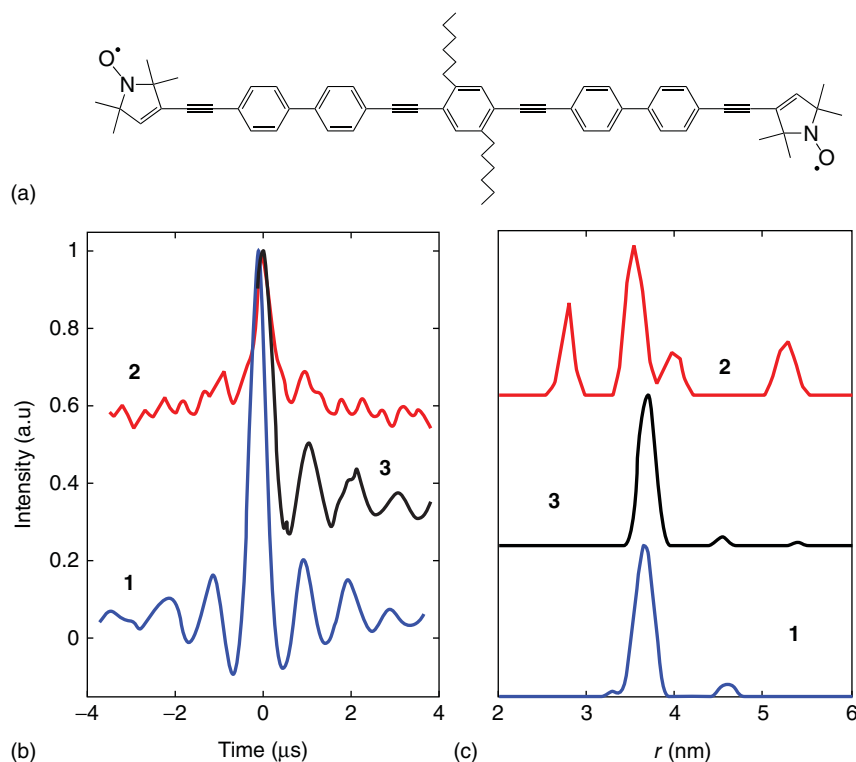


Figure 20.12. (b) X-band broadband SIFTER (1); rectangular pulsed SIFTER (2); and four-pulse DEER (3) – all measured at 50 K on the rigid nitroxide biradical in (a). The plotted data are background corrected and normalized to unity. For rectangular pulsed SIFTER, $\pi/2$ pulse was 8 ns; for four-pulse DEER, $\pi/2$ pulse was 16 ns, and pump pulse of 14 ns was applied at 70 MHz offset at the center maximum. (c) Distance distributions for corresponding time traces (1–3) produced by Tikhonov regularization included in DeerAnalysis 2013 software suite. (Reproduced with permission from Ref. 73. © Elsevier, 2015)

With pulses available, the outcome while encouraging was less convincing. Nevertheless, the improvement at Q-band was apparent as the time-domain data were much closer to DEER as compared to the case of low-power rectangular pulses shown in Figures 20.12(b,2) and (c,2).

Broadband SIFTER with adiabatic pulses has provided distance distributions of comparable quality to the four-pulse DEER (Figures 20.12b, 1 and 3; 20.12c, 1 and 3). The experimental results for SIFTER are thus generally encouraging. Systems with shorter distances, high local concentrations, and short relaxation times (e.g., membrane proteins) as well as short distances (<2.5 nm) may continue present a challenge. These cases, however, are handily addressed with DEER and DQC pulse sequences, which are far more robust techniques at present.

20.5 OTHER SINGLE-FREQUENCY PDS METHODS

20.5.1 Different Types of PDS Experiments

In a PDS experiment, first-order coherences are created for one or both spins, usually with a $\pi/2$ pulse followed by a pulse sequence that produces, after time $2t_m$, an echo that is used to sense the dipolar interactions. In Section 20.2, we outlined two types of PDS experiment, i.e., *single-resonance* and *double-resonance*, where we showed that the key difference between them is in how they evolve the dipolar coupling. Clearly, there is greater flexibility in manipulating pulse sequences in double resonance. In addition, it is possible to avoid certain artifacts that complicate single-resonance methods, viz. nuclear

ESEEM and sometimes relaxation effects, and also problematic are spurious dipolar trajectories, with only the DQC-6 and JB sequences able to successfully address them. Traditionally, double-resonance and single-frequency PDS methods were considered as distinct. However, our discussion and subsequent analysis in Section 20.2 indicated that double resonance is different from single-resonance more significantly in the manner in which it is conducted rather than in using pulses at a different frequency. For example, we have mentioned single-frequency methods of light-driven DEER and RIDME, neither of which use MW pulses for pumping, but they are otherwise conducted much like three- or four-pulse DEER acting (predominantly) on spins at a frequency different from that of the detected spins.

We now list several single-frequency methods, some are pure single resonance, while others function as double-resonance, but all are conducted at a single-frequency vis-à-vis MW pulses.

20.5.2 Single-frequency Single-resonance Methods

20.5.2.1 DQC Family

In addition to the DQC-6 pulse sequence described in Section 20.3, there are four- and five-pulse DQC sequences of the DQF COSY type, of which the latter is a constant-time sequence.²¹ They are currently not in use as DQC-6 is a far better technique. Furthermore, in addition to DQC-6, as already described, there is a variant used in the so-called DQM (double-quantum modulation) mode.⁸⁶ This is not a constant-time sequence; therefore, it entails relaxation decay and stronger ESEEM, which is addressed by adjusting the pulses.⁷⁹ However, similar to variable-time DEER,²⁵ it may produce stronger signals at an earlier time. DQC-6 has also been used in a DQ-filtered refocused PE mode, DQF-RPE.⁶⁹ This is essentially the recording of $\cos(at_m)$ as one would have with just RE, but the background is better suppressed.

20.5.2.2 Spin-correlated Radical Pairs

There are several such examples when dipolar spectroscopy was performed on light-induced transients, especially the case of SCRPs.^{59,87,88} A laser pulse creates nonequilibrium spin populations that contain dipolar order. Subsequently, a two-pulse sequence is

used with the first pulse being a $\approx\pi/4$ pulse that converts this dipolar order into antiphase coherence, and then it evolves in a refocusing sandwich to produce an out-of-phase echo (Figure 20.13).

The detection part of the JB sequence is similar to the sequence used to generate an out-of-phase echo in SCRPs, which is 90° out-of-phase to a normal PE. The initial nonequilibrium population of radical pair spin states gives rise to dipolar order $2\hat{S}_{1z}\hat{S}_{2z}$ with some amount of $\hat{S}_{1z} + \hat{S}_{2z}$ also present. If we consider weak dipolar coupling, the evolution is the same as that described in Section 20.4.4; therefore, only the reconversion part of the evolution of $\sin at_2$ is available, leaving the researcher with an antiphase Pake doublet. This is a true single-resonance case, but the practical role is limited to systems where reasonably long-lived SCRPs are generated and are amenable to PDS measurements. ZQC is also photo-produced in this case and can be refocused to evolve into observable single-quantum echo.

20.5.2.3 Out-of-phase Echo

An equilibrium spin state could itself entail dipolar order, e.g., at low temperatures and high fields due to the greater importance of higher-order terms in the density matrix expansion, leading to results similar to SCRPs, but one can use any bilabeled molecule with acceptable relaxation properties. Nitroxides are certainly included. An experiment⁸⁹ has been conducted recently at G-band (180 GHz) at 6.4 T and 5 K, where the spin system is highly polarized. The experiment could have been an out-of-phase echo as with SCRPs, but (as the spectrum was not too narrow) was performed instead as out-of-phase PELDOR to benefit from the absence of relaxation decay and zero dead time. This certainly is not necessarily an optimum experiment in terms of spin sensitivity and is not suited for the MW frequency range but is an interesting approach, nevertheless.



Figure 20.13. Out-of-phase echo can provide distances from $\sin(a\tau)$ evolution of the antiphase coherence produced with a $\pi/4$ pulse from the dipolar order formed in a spin-polarized SCRPs

20.5.3 Single-frequency Double-resonance Type Methods

20.5.3.1 '2+1' and Refocused '2+1' Sequences

The first useful PDS EPR technique was, as previously noted, the three-pulse DEER (PELDOR), which is a *double-resonance method*. Early DEER experiments made use of two MW power sources tuned to different frequency modes of a bimodal MW cavity resonator, as low-Q cavities were inadequate.¹¹ This was later addressed by Bruker with more efficient single-mode broadband split ring and dielectric resonators conveniently housed in flow cryostats.^{62,90–93} Before this happened, the '2+1' technique was introduced.^{3,94} It used one or two MW power sources operating at the same or close frequencies utilizing a standard TE₀₁₂ resonator. The pump pulse was generated at the same frequency (unlike DEER) but with an independent frequency source (like DEER). This was suitable for a typical pulse spectrometer and the technique was used in several studies¹⁵ despite several significant shortcomings. Applications that have benefited from the '2+1' method were cases of relatively narrow EPR spectra, such as the tyrosyl radical encountered in the study of photosynthesis or other radical cofactors, and the method was extensively applied to map the location of radicals in photosystems¹⁵ before the technique went out of use.

We note that '2+1' has a short but finite dead time. It is interesting whether this sequence with so much in common with DEER could be modified into a dead-time-free four-pulse '2+1' as was done to three-pulse DEER. Such a sequence was tested for this article. It turns out that the problem with the finite dead time in '2+1' cannot be as easily overcome by the addition of the refocusing pulse as in four-pulse DEER. With such a revision (Figures 20.1 and 20.14), one observes the same four dipolar trajectories as in four-pulse DEER,²² i.e., two signals $V_1(t)$ and $V_2(t-\tau)$ of which V_2 has zero dead time and their counterparts appear reversed in time, $V_3(T-t)$ and $V_4(T-t+\tau)$. Here, $V_k(t) = V_0[1 - p(1 - \cos at)]$ is a standard signal in DEER. However, unfortunately, the intensities of these 'dipolar pathways' are different for the two cases. Both types, zero- and nonzero dead time, are comparable in the modified '2+1'. In both cases shown in Figure 20.14, the incoherent pump pulse from a DEER oscillator was used. The hard pulses had a B_1 of 45 G. The performance of the '2+1' sequence in this setup is quite good, but it does not

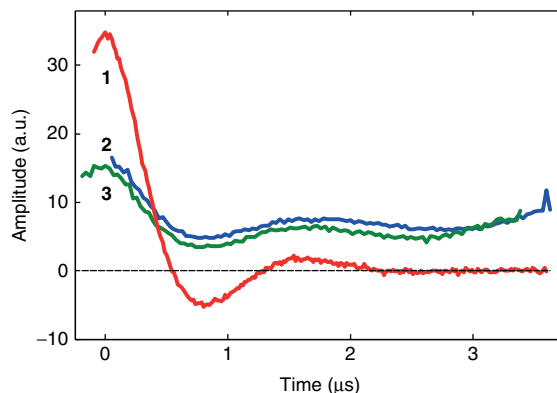


Figure 20.14. Measurements with '2+1' pulse sequence at K_u band based on intense pulses (2). Also plotted for comparison data (3) for '2+1' modified by adding a refocusing pulse in the same manner as in the standard four-pulse DEER or five-pulse RIDME to achieve zero dead time in dipolar evolution. The raw six-pulse DQC data (1) are shown for comparison on a common scale. All measurements were taken in succession with the same receiver gain and plotted as recorded using a reversed timescale to look as in standard DQC or DEER. The identical pump and detection frequency in all cases was 17.3 GHz, and $\pi/2$ and π pulses were 2 and 4 ns, respectively. The measurements were conducted at 60 K on a 15- μ l sample of 35 μ M of T4L doubly labeled with MTSL at 44 and 144 positions prepared in Tris-HCl buffer containing 30% w/v glycerol (this lab, previously unpublished)

reach the performance of DQC-6 conducted on the same sample for reference to provide a feeling for why such newer coherent methods are superior.

20.5.3.2 The RIDME Experiment

The simplest single-resonance PDS experiment is based on a PE, but extracting dipolar coupling is rarely possible, as it is masked by larger effects. A successful solution was DEER, but alternatives were also developed, viz. DQC and SQC techniques described such as DQF-COSY and DQC-6,^{20,21} but also three-pulse RIDME.⁹⁵ RIDME relies on spin flips caused by relaxation rather than by a pump pulse. Therefore, it may involve all the B-spins (i.e., those coupled spins not observed) independent of how wide the spectrum could be, thus, making it advantageous for, e.g., metal ions. The initial form of RIDME had the second refocusing pulse in a PE split into a $\pi/2 - T - \pi/2$ sequence, essentially producing a stimulated echo

(SE) sequence, $\pi/2 - \tau - \pi/2 - T - \pi/2 - \tau$ -echo with a long enough T to ensure relaxation of the B-spin to complete. By repeating the experiment with two values of T (short and long), it was possible to factor out the dipolar signal by dividing two traces, in one of which with long T spin–lattice relaxation caused a spin flip, thus substituting for a pump pulse. The efficiency of a relaxation flip was sufficient to produce clear dipolar modulation well above the level of residual postrefocusing effects.⁹⁵ The performance could be further improved if the coupled spin has a broader spectrum and shorter spin–lattice relaxation time T_1 than the observing spin A, making the spin B contribution dominant. A more sensitive A-spin (e.g., nitroxide) can be used to form the echo. Further pulse-sequence developments soon followed, reducing dead time by adding a fourth refocusing pulse²⁷ and then eliminating dead time altogether with the addition of one more refocusing fifth pulse as was done in four-pulse DEER,²⁶ although three-pulse RIDME is still in use with high-field high-frequency (HFHF) EPR.³⁸ These elaborations yielded a ‘2+1’-like, and its refocused version type, single-frequency sequences, but the pump pulse was replaced with the storage period $\pi/2 - T - \pi/2$ providing a variety of opportunities to invert the coupled spin with a broad spectrum and reduce some of the unwanted effects. These effects include nuclear ESEEM, spectral diffusion, unwanted dipolar signals of the ‘2+1’ type, and dipolar frequency harmonics for high spin. Several approaches have been tested to reduce unwanted effects, especially ESEEM from deuterium typically used in PDS for increasing T_m to improve the sensitivity and distance range. This includes conducting the experiment using two different T 's or at two temperatures, using Q-band as well as using soft pulses at Q-band.²⁹

RIDME as a pump pulse-free scheme is particularly valuable in relaxation-based single-frequency experiments, when most of the coupled spins are that of a metal ion, thus predominantly at a different frequency than the observed one, but it was also applied to nitroxides, where this is not the case.

Dead-time-free RIDME⁴⁴ (Figure 20.15) is an important development and was used in several studies on metalloproteins.^{29,30,38,44} It would be too difficult to pump the broad spectral extent of an ion, but relaxation accomplishes this task very efficiently. The maximum pump efficiency of 0.5 is due to the fact that this is relaxation, not population inversion by a pulse that could ideally flip all spins. The use of relaxation has peculiarities for high spins, where relaxation involving all

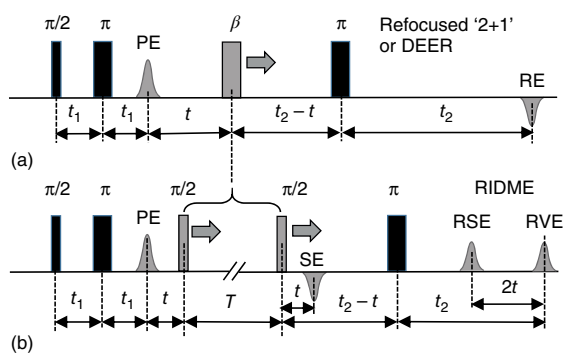


Figure 20.15. (a) Refocused ‘2+1’ sequence (or four-pulse DEER) can be transformed to the RIDME sequence by replacing its β -pulse with a period T of longitudinal storage. Note that, unlike in DEER, the β -pulse in ‘2+1’ is not a π -pulse in order not to suppress RE. (b) A single-frequency RIDME pulse sequence includes a pulse block $-\pi/2 - T - \pi/2 -$ to store coherences as z -magnetization; operate on it; and then transform to transverse coherence for detection. While this block is used in the same manner as a B-spin-flipping pulse, this function and the nature of coherence pathways and detected echoes are different than in (b). A refocused virtual echo (RVE), whose position is fixed in time is typically sampled, but the use of a refocused stimulated echo (RSE) was also reported. All spin manipulations that occur during the storage period T are aimed to flip the coupled spin, giving rise to other methods than RIDME

levels can produce $\Delta m_B > 1$, leading to harmonics of the dipolar frequency, so this should be addressed in distance reconstruction.^{28,96}

The sequence is used in five-pulse constant-time dead-time-free mode, i.e., using RE as a detection pulse sequence and a composite propagator $\pi/2 - T - \pi/2$ to make a storage period for relaxation-based spin pumping. However, there are principal differences here from detecting RE with no interfering pump pulse. As the sequence is of the double-resonance type, it cannot use pulse timing of a single-resonance five-pulse SQC sequence keeping the sum of refocusing sandwiches fixed. Instead, it uses four-pulse DEER timing, with the pump pulse block scanned between the last two pulses of RE sequence. This produces a refocused SE (RSE) and refocused virtual echo (RVE), separated by $2t$, where t is the evolution variable. Both can be used, the latter is usually preferred, but each is half of the RE intensity for the same t_m . Note that five-pulse SQC does not form SE, both RSE and RVE collapse into RE at $t = 0$.

Therefore, the storage block is just a delay in SQC-5 in the absence of phase relaxation whose existence is necessary for this propagator to attain its purpose. Moreover, pumping B-spin during storage is basically of no use for SQC-5, as it is truly different from double resonance in dipolar evolution.

As for using moving pulses at the detection frequency, there are several artifacts; particularly, nuclear ESEEM issues have to be addressed for deuterium. This was investigated²⁹ as we previously noted and the referencing was made based on using different temperatures, soft pulses, and different durations of storage period. In such methods, ‘pumping’ on detected spins (A-spins) produces artifacts, so this is undesirable.^{3,22,40} And when they are intentionally applied to operate on detected spins (e.g., RIDME on nitroxides), their performance has not been yet as convincing as that of standard robust techniques such as DEER or DQC due to artifacts and significant loss of signal.

All in all, the use of a storage propagator is enabling approaches to improve sensitivity in the case of broad spectra of metal ions, for which there are few alternatives, and in addition, it offers a variety of methods to flip B-spins other than by relaxation in RIDME. That is, one can use other suitable means that can change the dipolar coupling – e.g., light pulse, electron beam, relaxation, chemical reaction, or some other process that can change polarization or create, modify, or remove spin density.

20.5.3.3 Field-jump PDS Experiment and Its Modern Analogs

Another example of single-frequency dipolar spectroscopy is the field-jump (FJ) DEER experiment based on a $(\pi/2)_A - \tau - (\pi/2)_A - T - (\pi/2)_A - \tau$ -echo-stimulated echo (SE) pulse sequence with the pumping of a different spectral region performed during the $\pi/2 - T - \pi/2$ storage period.^{27,38} It does not require a different frequency source to pump, but a field jump or sweep produced by a current pulse is utilized to make the equivalent of pumping B-spins at a different spectral region or creating an adiabatic population-inversion pulse⁴¹ using a long MW pulse and a field sweep in a collective action during the storage period, thereby presenting a rather complex propagator, which flips spins at different spectral regions, as does DEER. The pulse sequence, however, was exercised as SEDOR,³⁸ i.e., by advancing pulse sequence length similar to PE

or RE. The method entails phase relaxation decay and nuclear ESEEM issues. Signal referencing, resembling RIDME, was utilized to remove most of ESEEM and to account for relaxation decay. The dead-time issues were partly mitigated by adding a fourth refocusing pulse to the stimulated-echo sequence used. The four-pulse sequence resembled ‘2+1’ with a pump pulse replaced with a $\pi/2 - T - \pi/2$ magnetization storage period and all the pumping being located there. However, the constant-time sequence mode was not used. Recent rethinking of the field sweep approach produced an experiment dubbed CIDME (chirp-induced dipolar modulation enhancement), which uses frequency-chirped adiabatic MW pulses⁴⁰ instead of magnetic field sweep for population inversion. However, it also adds a fifth pulse²⁶ enabling zero-dead-time implementation based on the scheme developed and now routinely employed with the latest RIDME technique discussed earlier. It was shown that for nitroxides it could be beneficial for low-power spectrometers as the adiabatic pulse could be long but without delay effects (see Section 20.6.5).

20.5.3.4 Laser-induced DEER

There are more single-frequency PDS experiments known; however, some (or most) of these single-frequency methods are actually double resonance. This includes laser-induced PDS,⁴³ which can use a high-Q single-mode resonator and provide pump action optically by effecting a change in spin polarization, e.g., by optical generation of a porphyrin triplet with a laser pulse. With a short enough optical pulse, it is possible to access a shorter range of distances than in standard DEER, especially if the detection pulses are made as intense as in DQC. A triplet-state EPR spectrum is much wider than that of a nitroxide, so there are relatively few molecules in the triplet state at the same frequency as a nitroxide, which will otherwise contribute ‘2+1’-like type spin dynamics as noted in Section 20.5.1. Therefore, it is still a double-resonance experiment, even though no MW pulses at the second frequency are needed. In addition, refocusing and pulse evolution (fixed detection sequence) are particularly in line with a double-resonance (DEER) approach. The only potential issue is the quantum yield, as it is desirable that at least 10% of the nitroxides have their partner with its spin flipped.

20.6 2D-FT ORIENTATION-CORRELATION PDS

20.6.1 Orientational Aspects in PDS

The primary goal of any PDS experiment is to determine distances between electron spins. The outcome could be affected by the fact that the time-domain signal recorded in a PDS experiment can be sensitive to orientations of the coupled magnetic dipoles in the molecular frame, which gives rise to effects known as orientation selection or correlation⁹⁷ (see also Chapters 11 and 19). In the fully isotropic case for a pair of coupled electron spins for each interspin orientation of the vector \mathbf{r}_{12} connecting the spins, all orientations of \mathbf{r}_{12} relative the static field \mathbf{B}_0 are described by the polar and azimuthal angles θ and φ and are equally probable, e.g., for two point dipoles. The dipolar coupling then depends only on θ as $(3\cos^2\theta - 1)$, and this gives rise to the characteristic dipolar line shape (Section 20.2.2) known as a Pake doublet.^{49,50} However, for a spin label the orientation of the spin-bearing moiety may be fixed and tilted relative to \mathbf{r}_{12} if it is not flexibly tethered. The EPR spectra in solids are determined by the hf and \mathbf{g} -tensors whose anisotropies are defined in their respective principal frames. (The hf and \mathbf{g} -tensor principal frames may not necessarily coincide, but in the case of nitroxides, the differences are typically small and can largely be ignored.) The orientations $\Omega_k = (\alpha_k, \beta_k, \gamma_k)$, $k=1, 2$ of these frames are then defined relative to \mathbf{r}_{12} taken as the polar axis giving five independent Euler angles with $\alpha_1 = 0$.⁶⁵ Nearly always, the finite pulses in PDS excite only a fraction, frequently a small fraction of the EPR spectrum; this particularly is true at high fields where EPR spectra are often dominated by the \mathbf{g} -factor anisotropy.³⁸ Therefore, in cases of pronounced anisotropy with well-defined orientations of the magnetic frames relative to \mathbf{r}_{12} , each \mathbf{r}_{12} orientation selects a range of orientations in \mathbf{B}_0 and consequently a subset of possible dipolar couplings, so that the dipolar spectrum no longer has the shape of an ideal Pake doublet. Thus, PDS experiments at high fields, which are usually DEER or RIDME^{28,38,40,44} type double-resonance experiments, could be very sensitive to molecular orientations and can be explicitly directed toward obtaining additional details of molecular structure.

Our focus will be on nitroxides as they have been used in most studies. One expects less pronounced

orientation effects (correlations) as well as a greater relative contribution of hf tensor anisotropy as compared to the \mathbf{g} -tensor at fields up to Q-band. This is certainly the case for nitroxide spin labels, where such effects are not highly pronounced and would require magnetic frames of electron spins to be well fixed relative to the molecular frame. Typically, nitroxide spin labels exhibit low anisotropy because their flexible side chains give rise to several rotamers.^{98,99} Nevertheless, orientation correlations were revealed by conducting DEER experiments from X to Q band using several pump and detection frequencies over the EPR spectrum. This could be a very time-consuming endeavor.

20.6.2 2D-DQC Correlation Maps

The standard DQC-6 experiment under nonselective spectral excitation is focused on accurate distances and suppresses the manifestation of orientational effects in the dipolar evolution signal, as the spins of molecules at all orientations relative to \mathbf{B}_0 contribute equally to the signal. This ideal picture of eliminating the orientation effects in the DQC-6 experiment is limited by the finite nature of the pulses. (The contribution of the flip-flop terms in the secular part of the dipolar spin-Hamiltonian depends on the orientationally dependent frequency separation between spectral components underlying the spectrum. However, these effects are usually relatively small unless the coupling becomes strong, i.e., at distances as short as 1.0–1.5 nm.) The dipolar evolution is acquired as the amplitude of the spin echo, i.e., each at refocusing point; thus, there is no dependence on frequency offset. Nevertheless, the spin-echo envelope, determined by the EPR spectrum shape, does encode the information on orientations of the magnetic frames of coupled electron spins, enabling an orientation selection 2D-DQC technique. This hidden orientational information can be revealed if one elicits the contributions to the full dipolar signal made by each spectral component contributing to the spin-echo signal. This is revealed by taking the Fourier transformation (FT) of the spin-echo shape, providing the EPR spectrum, and enabling a 2D-FT plot of the dipolar spectrum vs the rigid-limit nitroxide spectrum, each point of which corresponds to a set of molecular orientations. This yields a 2D-FT frequency correlation plot, which is a fingerprint of the orientation-dependent effects caused by the anisotropy of magnetic tensors. In the actual

DQC experiment, the full echo envelope is captured by a fast ADC, sampling at GHz rates and can be stored for 2D processing. (For further FT techniques, see Chapter 15.)

Assuming ideal pulses, the dipolar signal relevant for 2D-DQC experiment can be written out. For spin 1, antiphase coherence $2\hat{S}_{1x}\hat{S}_{2z}$ produced after the DQF by the $\pi/2$ pulse 5 evolves into observable in-phase coherence in the last $t_2 - \pi - t_2$ sandwich ($t_2 = t_m - t_p$) as

$$2\hat{S}_{1x}\hat{S}_{2z} \rightarrow (\hat{S}_{1y} \cos \Delta\omega_1 \delta t - \hat{S}_{1x} \sin \Delta\omega_1 \delta t) (s_{t_2} c_{t_2+\delta t} + c_{t_2} s_{t_2+\delta t}) \quad (20.29)$$

Here, δt is the time variable taken from the refocusing time $2t_2$. After adding to equation (20.29), the dipolar evolution phase $\sin at_p$ acquired through the evolution in the preparation period before the filter, the detected in-phase component in equation (20.29) is

$$\begin{aligned} & \hat{S}_{1y} \cos(\Delta\omega_1 \delta t) \sin(at_1) \sin(at_2 + a\delta t/2) \\ &= \hat{S}_{1y} \cos(\Delta\omega_1 \delta t) \sin(at_p) \sin(at_m - at_p + a\delta t/2) \\ &= \hat{S}_{1y} \cos(\Delta\omega_1 \delta t) \cdot [\cos(at_x - a\delta t/2) \\ & \quad - \cos(at_m + a\delta t/2)] \end{aligned} \quad (20.30)$$

For the second spin, $\Delta\omega_2$ is replaced by $\Delta\omega_1$, but the dipolar part is the same. We now define the spin-echo time $t_{\text{echo}} \equiv \delta t$ and the dipolar evolution time $t_{\text{dip}} \equiv t_x$ variables, and also $t_{\text{dip}}' = t_{\text{dip}} + t_{\text{echo}}/2$. The 2D signal $F(t_{\text{echo}}, t_{\text{dip}}')$ is in terms of these variables. After a 2D FT, followed by a shear transformation of the frequency variables,⁶⁵ a 2D-FT plot $V(v_{\text{echo}}, v_{\text{dip}})$ is produced. The resulting 2D plot (or map) gives the dipolar spectrum for each frequency in the spectrum. Figure 20.16(a) and (b) shows examples of such distinctive 2D maps simulated for uncorrelated and strongly orientationally correlated cases. On the side of the plots are the spectral sums calculated along v_{dip} and v_{echo} . They give, respectively, the 1D EPR spectrum (with no dipolar effects in it) and the pure the 1D dipolar spectrum (Pake doublet without the orientation effects), as for any spin all its partners contribute to the sum, so all orientations contribute equally.

In Figure 20.16(c), we show the 2D DQC data obtained at 17.25 GHz and 60 K on 15 μl of 15 μM solution of a 3-nm rigid rod biradical²¹ in *o*-terphenyl- d_{24} glass. The shortest π pulse available for a sample of this size was 4 ns, yielding a B_1 of 45 G. Yet, this B_1 is insufficient to provide *completely* uniform spectral coverage for the whole ^{14}N nitroxide spectrum. However, this is not a very serious problem. As most of the spectrum is covered, the outcome can be simulated

for the finite B_1 used.⁶⁵ In addition, one could increase the B_1 to ≈ 60 G using a somewhat smaller resonator. Nevertheless, two separate data collections were made to widen the coverage. The pulse sequences were applied 30 G apart at the low- and high-field parts of the spectrum, respectively. The individual 2D spectra were then truncated on opposite sides at a selected frequency and combined into the single spectrum shown in Figure 20.16(c,2). This manipulation is not absolutely necessary, as fitting each of the 2D spectra suffices to reveal the key orientational properties. This approach based on recording two spectra does not incur a significant penalty in acquisition time, as most of it is used to produce good SNR for the high-field side of the spectrum, which has a factor of ≈ 3 lower intensity than the more intense central and low-field regions.

For this nearly linear biradical, the nitroxide moieties have their beta angles, $\beta_{1(2)}$ at about 90° relative to the interspin vector, r_{12} , connecting the points located at three-fourth of the NO bond length toward the nitrogens. As confirmed by simulations, the remaining angles are relatively unimportant. Molecular modeling²¹ has determined $|r_{12}| = 2.89$ nm and the following set of Euler angles: $\Omega_1 = (0^\circ, 75^\circ, 0^\circ)$, $\Omega_2 = (90^\circ, 111^\circ, 0^\circ)$.^{21,22} We show in Figure 20.16(c) the correlation maps for experimental and calculated data, rendered as normalized filled contour plots. The plots are quite similar, i.e., nitroxide orientations are of the expected type as simulated in Figure 20.16(b), but there are some visible differences that could be addressed by modeling. One may also need to account for the effects of the resonator bandwidth, which would require more substantial computational efforts than used in this work. In summary, we note that acquiring orientational information by DEER necessitates recording several traces,¹⁰⁰ whereas 2D DQC can do it in a single pass (or just two). The outcome is not the full equivalent of ideal hard pulses but is deemed to be close enough in information content as we have shown above. However, DEER, to its advantage, is not limited to just nitroxides and can be applied to infer orientational information from very broad spectra of metal ions and at high fields from orientationally better resolved spectra.¹⁰¹ It is, however, worth mentioning that the 2D-DQC technique, as for the 1D-DQC on which it is based, presents a robust sensitive and low-artifact technique covering three octaves in distance (i.e., a factor of ≈ 500 in dipolar frequency). The upper range of distances is limited by the phase memory time T_m

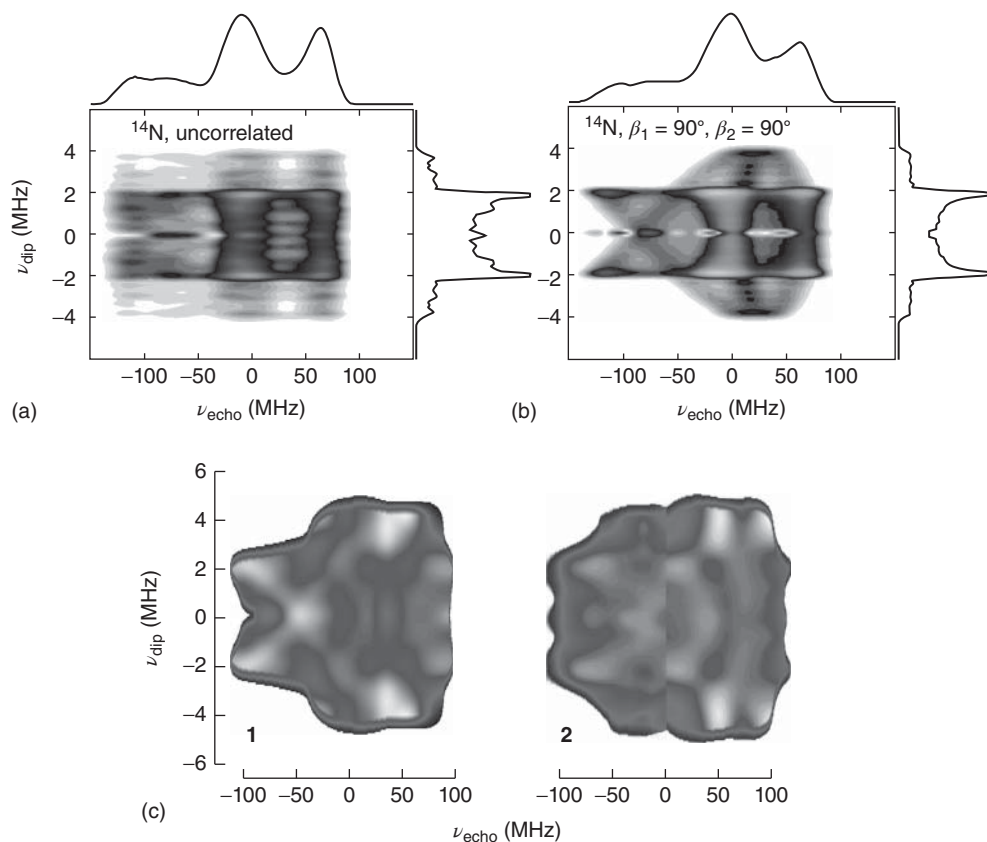


Figure 20.16. Illustration of the 2D-DQC experiment: (a, b) Simulated 2D DQC magnitude filled contour plots obtained by 2D FT with respect to t_{dip} and t_{echo} . Shown are uncorrelated (a) and correlated (b) cases for $B_0 = 6200$ G and $\nu_{\text{dip}} = \omega_{\text{dd}}/2\pi \approx 2$ MHz ($r_{12} = 2.96$ nm). B_1 was set to infinity (i.e., assuming perfect delta-function pulses), pseudosecular terms were neglected. In (b) Euler angles beta (polar to r_{12}) were $(90^\circ, 90^\circ)$ corresponding to strong correlations. The remaining Euler angles were set to zero. The side plots are a Pake doublet (on the right) and 1D EPR absorption spectrum from dipolar broadening (at the top). Both were produced by summing the 2D signal along the orthogonal frequency dimension. (c) Experimental (2) and calculated (1) 2D correlation maps from 17.25 GHz DQC data. Map (2) is composed of two correlation plots obtained from 2D data acquired for MW pulses applied at 28 and -56 MHz frequency offsets from the central maximum of the ^{14}N nitroxide EPR spectrum. The cutoff line for each map is at the offset of -42 MHz. Map (1) was computed using B_1 of 80 G, $r = 2.9$ nm, and the set of Euler angles $\Omega_1 = (0^\circ, 75^\circ, 0^\circ)$, $\Omega_2 = (90^\circ, 111^\circ, 0^\circ)$ from molecular modeling. (Reproduced with permission from Ref. 22. © Springer, 2014)

and can reach ≈ 8 nm or likely more in deuterated systems. DEER was shown to reach beyond 10 nm in fully deuterated systems or even more in special cases.¹⁰²

20.6.3 Perspectives for 2D-SQC

The same type of experiment can be conducted using SQC sequences of Section 20.4, but it would take a much larger effort to isolate the dipolar part of

the signal for most of them. The least effort is expected for the JB sequence due to good background suppression, although we do not expect significant differences from DQC as the nature of the signal is similar. The performance of the rest of the SQC sequences described in Section 20.4 needs to be improved by using B_1 's even greater than 45 G. Such high B_1 's can be combined with more uniform broadband excitation from amplitude-modulated pulses, such as

Hermite pulses.¹⁰³ Alternatively, the use of moderate B_1 frequency-chirping quasi-adiabatic pulses could help to suppress unwanted dipolar signals^{73,84} and reduce backgrounds, although such techniques (see next section) in 2D format are yet to be developed to the extent comparable to routinely performed 2D-DQC, as coupled spin dynamics is more complex with adiabatic pulses and the time dispersion in dipolar evolution limits the strength of the dipolar coupling that can be faithfully reconstructed by this approach.

20.6.4 2D-SIFTER

With the advent of frequency-swept (chirp) quasi-adiabatic pulses in EPR, this approach has been applied to improve SIFTER (see Section 20.4). Recent work has applied chirped-pulse SIFTER approach to provide the 2D mode in the manner of 2D-DQC. We comment on specifics of this new method. For each contributing spin, the time of pulse excitation depends on its frequency offset and the (inverse) rate of sweep, $k = (df/dt)^{-1} \approx \Delta t_{\text{pulse}}/\Delta f$, where Δf is the sweep range and Δt_{pulse} the pulse width. This results in a time dispersion of Φ_{off} , spreading the echo. The problem was solved for PE by Böhlen *et al.* using a 2:1 chirping rate scheme for pulse k 's ratio.⁸⁵ For RE, a 2:2:1 scheme is efficient⁷³ (see also the following section). For coupled spins, situated at different offsets, excitation is applied at different times. While spin dynamics in this case is quite complex, for weak coupling, we can employ a model based on the simplified picture of two hard pulses, each acting on its spin when the frequency is equal to the spin resonance frequency. This allows a qualitative treatment to be made, illustrating the specifics of this approach. We can employ the methods for tracking dipolar pathways outlined in Section 20.2, as was developed for DEER with multiple pulses (excitations) at the pump frequency.²² We show in the following section an example sketched for chirp-RE to illustrate the evolution of dipolar coupling.

In Figure 20.17(a), the chirp pulses are depicted in the second row as a 2:2:2:1 inverse sweep rate scheme.⁸⁴ As in the Böhlen–Bodenhausen 2:1 scheme,⁸⁵ only the last π -pulse needs to have a faster rate to refocus offsets without phase dispersion. The evolution of dipolar phases for spins S_2 and S_1 experience CT by the $(\pi/2)_y$ pulse. The switching occurs in two steps. One of the two spins, S_1 that started evolution later than the other, passes through

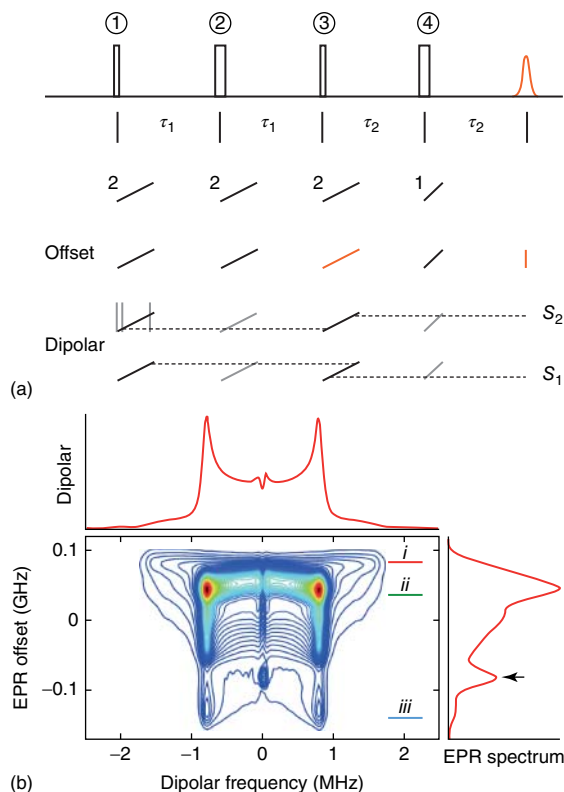


Figure 20.17. 2D-SIFTER with adiabatic pulses. (a) Under the standard rectangular-pulse sequence, the pulse sequence with frequency chirping pulses is shown as each pulse frequency vs time. The 2:2:2:1 inverse chirp rate ratio scheme is employed. The chart under this graph shows timing of pulse action on offset progression (creation, refocusing), essentially replicating the pulse frequency ramps (red lines indicate PE from pulses 1, 2 and RPE; $(\pi/2)_y$ pulse has no effect on refocusing offsets). For two coupled spins 1 and 2, their dipolar evolutions are charted with spin 2 shown starting first at the low-frequency path. At the third $(\pi/2)_y$ pulse, there is coherence transfer (CT) between the spins. For spin 2, the gap in dipolar evolution is produced in CT to spin 1 as the state of the dipolar order existed between the spins, when they waited for the transfer to complete. An overhanging trajectory is observed in the delayed path starting at the higher frequency on spin 1; in this case, it corresponds to a period of evolution as DQC/ZQC. These gaps are equal and do not contribute dipolar evolution; the offsets are exchanged but refocusing is unaffected. This pulse is skewless as the dipolar variable, $t_x = \tau_1 - \tau_2$ does not depend on frequency offsets. (b) The correlation map of the 2D-DQC type, as shown in Figure 20.16. The cross-sections at spectral points i–iii are available in Ref. 84. (Reproduced with permission from Ref. 84. © Royal Society of Chemistry, 2016)

DQ and ZQ coherence orders, whereas its partner passes through dipolar order. There is no effect on evolution of offsets, as they simply continue as if CT had not happened, so the offsets behave as in RPE (see the following section). Out-of-phase components caused by pulse imperfections and those that can be produced, e.g., by Bloch–Siegert phase shifts could evolve differently, and pseudosecular terms can contribute more issues. These effects could be studied numerically. Overall, there is enthusiasm that this four-pulse single-resonance 2D-method could work well for sufficiently weak couplings, starting from about 3 nm as was demonstrated. There is indeed good coverage achieved of the Q-band nitroxide spectrum, and the Pake doublet for the ≈ 3.5 nm distance in panel (b) does not show any problem.

20.6.5 Chirp-pulse RE: Evolution and Refocusing

For a standard monochromatic pulse, the effect of the pulse on the dipolar evolution given by the set of trajectories $\{\Phi_{\text{dip}}(t)\}$ in the detected signal can be calculated using the simple means of Section 20.2 based on dipolar evolution operators $\hat{D}(t)$. Chirp pulses (see Chapter 21) act on both spins at different times, so each pulse can be viewed as a double pulse acting first on \hat{S}_1^\pm of the first spin, changing \bar{p} to stay on the selected pathway and after a delay acting on $\hat{D}(t)$ of the second spin to modify the trajectory set. Assuming nearly adiabatic pulses, we can approximate their action by hard pulses separated by a delay. This does not multiply the pathways for π pulses but introduces $\Phi_{\text{dip}}(t)$ dispersion into echo-forming spin ensemble. The evolution of $\Phi_{\text{dip}}(t)$ will be reversed twice for a π -pulse introducing delay to $\Phi_{\text{dip}}(t)$'s. A $\pi/2$ pulse flips half the spins, thereby doubling the number of trajectories and delaying those flipped. The delay (phase shift) depends on the pulse frequency sweep rate and the offsets of the spins. We focus on dipolar evolution in RE and will consider this case here using as an example the sequence $\pi/2 - t_1 - \pi - (t_1 + t_2) - \pi - t_2 - \text{echo}$. The dispersion effects for adiabatic PDS sequences, such as shaped-pulse SIFTER, have been analyzed in the literature.⁸⁴

The sequence (Figure 20.18) is a 2 : 2 : 1 chirp RE described in the work on broadband SIFTER,⁷³ where the ratio is that of inverse frequency sweep rates, $(df/dt)^{-1}$. The PE in the Böhlen–Bodenhausen scheme⁸⁵ has

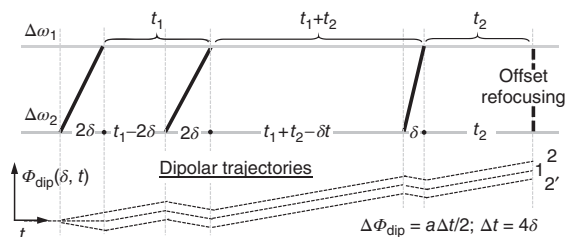


Figure 20.18. The RE pulse sequence based on adiabatic (frequency-chirping) pulses and the phase-invariant refocusing scheme with the (inverse) frequency sweep rate ratio 2 : 2 : 1. Each pulse has its frequency equal to spin offsets $\Delta\omega_1$ and $\Delta\omega_2$ at times shifted by 2δ (for the first two pulses) or δ (for the last π pulse). The pulse action is assumed to be that of two hard pulses positioned at the times when the pulse frequency equals the offsets. The first $\pi/2$ pulse produces two dipolar pathways with equal amplitudes, i.e., the two dipolar phase trajectories denoted 2 and 2'. Each refocusing π pulse introduces to the evolution of Φ_{dip} , a time lag equal to twice the time shift by reversing dipolar evolution twice during the pulse. The spin at $\Delta\omega_1$ has just one phase trajectory intermediate to 2 and 2' for $\Delta\omega_2$

inverse chirping rate ratio 2 : 1 to refocus the offsets without phase dispersion; and so does the 2 : 2 : 1 scheme for RE, as for any value of δ the refocusing occurs at time $2(t_1 + t_2) + 2\delta$ after the initial time lead of 2δ , so the refocusing point is at $2(t_1 + t_2)$ for all δ . The $\pi/2$ pulse first engages spin at $\Delta\omega_2$ and after a delay of 2δ another at $\Delta\omega_1$, flipping it with probability $p \approx 0.5$. This produces two dipolar trajectories 2 and 2', of which one whose evolution was reversed is delayed by 4δ , hence introduces $-2a\delta$ phase shift to Φ_{dip} . This picture repeats with each π pulse and is similar for the $\Delta\omega_1$ and $\Delta\omega_2$ pathways. We illustrate this point by calculating part of the evolution for trajectory 1 of spin 1 at $\Delta\omega_1$ to the point in time t after the end of the first π pulse. For the RE in Figure 20.18, the pathway to echo is $(-1, +1, -1)$. Referring time to the end of the $\pi/2$ pulse, we write the dipolar evolution as follows:

$$\begin{aligned} \hat{S}_1^- &\xrightarrow{t_1-2\delta} \hat{S}_1^- \hat{D}_{t_1-2\delta}^* \xrightarrow{\pi(\Delta\omega_2)} \hat{S}_1^+ \hat{D}_{t_1-2\delta}^* \xrightarrow{2\delta} \hat{S}_1^+ \hat{D}_{t_1-2\delta}^* \hat{D}_{2\delta} \\ &\xrightarrow{\pi(\Delta\omega_1)} \hat{S}_1^+ \hat{D}_{t_1-2\delta} \hat{D}_{2\delta}^* \xrightarrow{t} \hat{S}_1^+ \hat{D}_{t_1-2\delta} \hat{D}_{2\delta}^* \hat{D}_t \\ &= \hat{S}_1^+ \hat{D}(t_1 + t - 4\delta) \end{aligned} \quad (20.31)$$

We see that the π pulse introduced a delay 4δ to the evolution of the dipolar phase, as one expects for a ‘dipolar refocusing sandwich’ ($2\delta - \pi - 2\delta$). Full dipolar trajectories are shown in Figure 20.18; there are

two denoted as 2 and 2' for the 'lower' $\Delta\omega_2$ path, 2 but only one trajectory exists for the spin at $\Delta\omega_1$ (cf. Figure 20.18). Collectively, they produce a skew of $4a\delta$ which depends on the excited spectral shape and extent. For a 200 ns pulse, the skew could be as large as 400 ns. Assuming it to be ≈ 200 ns on average, and permitting the error in dipolar phase of a quarter period of dipolar oscillation, we estimate that distances less than 3.5 nm may be too short for such a pulse sequence. Nevertheless, for moderate and long distances this pulse sequence may be useful.

20.7 RELAXATION AND INSTANTANEOUS DIFFUSION

20.7.1 Instantaneous Diffusion

As we noted in Section 20.2.2, the intramolecular dipolar coupling is the main term in \hat{H}_{dd} . However, surrounding spins usually cannot be discounted. Considering intermolecular couplings leads to a secular dipolar Hamiltonian, where each spin k is in principle coupled to all N spins in the sample, so that \hat{H}_{dd} becomes

$$\hat{H}_{dd} = \sum_{n \neq k} a(\mathbf{r}_{kn}) (3\hat{S}_{kz}\hat{S}_{nz} - \hat{S}_k\hat{S}_n) \quad (20.32)$$

where $k, n \leq N$. In PDS, the flip-flop terms in equation (20.32), which could lead to spin diffusion, should be neglected to give just the secular part of dipolar coupling $\hat{H}_{dd} = \sum_{n \neq k} a(\mathbf{r}_{kn}) \hat{S}_{kz} \hat{S}_{nz}$. This certainly holds

for most cases, including nitroxides, unless the concentration is approaching the molar range, but other concentration effects impair the methods well before it is reached.⁹⁸ The upper level of concentration may become even less for cases such as trityl radicals or H-atoms, whose lines are narrow. This case may require the SLE treatment to account for relaxation caused by these terms.⁹⁹

As was shown by Klauder and Anderson⁵ and confirmed in a many-body analysis by Nevzorov and Freed,⁹⁹ the dipolar coupling in equation (20.32) leads to an inhomogeneously broadened line having a Lorentzian dipolar line shape. For a spin system at concentration C having hypothetically zero-width dipolar spectrum, applying a hard π pulse 'instantaneously' produces dephasing whose FT yields an inhomogeneous line width $k_0 C$, where $k_0 = 2\pi\mu_0\gamma_c^2\hbar/9\sqrt{3} \approx 10^{-3}\mu\text{M}^{-1}\mu\text{s}^{-1}$. This explains

the term of 'ID' applied to this case.⁵ In the primary spin-echo $\pi/2 - \tau - \pi - \tau$ -echo, if only a fraction p_A of spins is excited (flipped), i.e., the A spins, ID contributes to the echo decay as

$$V(\tau) = V(0) \exp(-p_A k_0 C \tau) \quad (20.33)$$

The signal decay appears as a relaxation decay but is based on coherent spin dynamics and therefore can be at least partially refocused.⁴⁸ ID affects single- and double-resonance pulse sequences differently. In DEER, pump pulses are applied to the B-spins, refocusing the dipolar coupling of A-spins with the B-spins; but the dipolar phase at the point of detection (i.e., the echo) depends on the varying position of the pump pulse, leading to time dependence in the echo. The (pumped) B-spins include the partner to an A-spin and all the surrounding spins at the frequency of the pump pulse. All these dipolar interactions of the A-spin with unaffected B-spins are refocused in the signal, which becomes a product

$$\begin{aligned} V(t) &= V_{\text{intra}} V_{\text{inter}} \\ &= V_{\text{intra}} \left\langle \prod_{n \neq 1,2} (q_B + p_B \cos a(\mathbf{r}_{1n})t) \right\rangle_{\{r_{1n}\}} \end{aligned} \quad (20.34)$$

where for partner spins 1 and 2, $V_{\text{intra}} = V_0(q_B + p_B \cos a_{12}t)$ is a standard DEER signal with p_B the probability to flip a B-spin and $q_B = 1 - p_B$. Markov averaging of V_{inter} in equation (20.34) produces,

$$V(t) = V_{\text{intra}}(t) \exp(-k_0 C p_B t) \quad (20.35)$$

where C is spin concentration in the (uniform) sample. Thus, equation (20.35) is an estimate of ID for the DEER experiment. For observing the RE sequence with a length of $2t_m$, ID from A-spins, whose excitation probability is p_A as in equation (20.33), contributes to the signal a constant factor of $V(t_m) = V(0) \exp(-p_A k_0 C t_m)$ with t_m in place of τ to give the total ID contribution to DEER: $V(t) = V_{\text{intra}}(t) \exp[-k_0 C (p_B t + p_A t_m)]$ (see Chapter 19).

Because single-resonance pulse sequences consist of refocusing segments, the static dipolar coupling to B-spins refocus in each of them. However, when relaxation cannot be neglected, B-spins contribute spectral diffusion to the dynamics of A-spins, leading to decay.^{1,98} Note that for ideal hard pulses there are no B-spins, but they exist for real nonideal pulses. The single-frequency techniques such as PE and RE do

contain an ID contribution from A-spins as

$$V(t_m) = V(0) \exp(-p_A k_0 C t_m) \quad (20.36)$$

However, modification of the RE sequence to form a PDS pulse sequence by inserting a propagator \hat{U} (see Section 20.2.7) contributes sequence-specific time dependence to the ID, as refocusing of coupling may be introduced by the nature of \hat{U} and may partially refocus ID.⁹⁹ Thus, equation (20.36) will now depend on t_x , such as contributed by the term in $\cos at_x$ in equation (20.23) and could introduce a slope to the background. The task of writing out this term rigorously is quite complicated for any PDS method,⁹⁹ as the accurate result also depends on generation of higher order coherences, flip-flop effects, and spectral diffusion – all constituting a many-body problem. It has been shown⁹⁹ that for a solid-echo there is a decay of the signal due to these MQCs. We estimate that for the *solid-echo-based* SIFTER sequence that refocuses ID at $t_x = 0$ (assuming an ideal $(\pi/2)_y$ pulse and not including higher order coherences) introduces a time dependence

$$V(t_x) \cong V(0) \exp(-pk_0 C |t_x|) \quad (20.37)$$

independent of t_m , which adds to the relaxation decay when it is significant, leading to strong attenuation of the weak signal at large t_x 's. Interestingly, the DQC-6 pulse sequence appears to have no such decay in t_x , as the ID term is constant and the same as in RE; that is,

$$V(t_x, t_m) = V_0(t_x) \exp(-pk_0 C t_m) \quad (20.38)$$

where V_0 is the signal in isolated pair. Generally, proper phase cycling does not modify ID, which otherwise would degrade the performance; this is the case with DQC-6. However, $(\pi/2)_x$ pulses do generate even higher order coherences with other spins, and as they are real pulses they also act to an extent as $(\pi/2)_y$ to generate odd coherence orders and causing refocusing, so one could also expect some dependence on the t_x variable.

20.7.2 Local Concentrations; Freezing Effects

If the sample is not uniform, $V_{\text{inter}} \approx \exp(-pk_0 \bar{C}_{\text{loc}} t)$ in DEER, where \bar{C}_{loc} is an effective local concentration, so from averaging over the sample volume the expression $\langle C_{\text{loc}}(\mathbf{r}) \exp(-k_0 p C_{\text{loc}}(\mathbf{r}) t) \rangle_r$, will possibly produce a more complex dependence than a simple exponential factor. A recent study⁷⁵ was conducted to determine the effect of adding glycerol to an aqueous

sample on the intermolecular decay (or ‘background slope’) in DEER for a spin-labeled protein. It showed an increase in \bar{C}_{loc} when the glycerol concentration was below ≈ 50 wt% and was typically decreasing with increasing freezing rate. Thus, caution needs to be exercised when estimating concentrations from slopes in DEER. It should not be forgotten that similar concentration effects are expected for single-resonance techniques, but they are of least concern for the methods that suppress background, such as DQC-6.

20.7.3 Fractional Dimension

When spatial distributions of spins are not locally isotropic, this can lead to time dependence in the ID term that is described by a stretched exponential with fractional dimensionality, α . Thus $V_{\text{inter}} \approx \exp(-p \bar{C}_{\text{loc}}^{(\alpha)} k_0^{(\alpha)} t^{\alpha/3})$.¹² This can correspond, e.g., to an amyloid fibril; a self-avoiding polymer chain containing randomly spin-labeled sites ($\alpha = 1$); or lipid bilayers, particularly liposomes ($\alpha = 2$). Usually, α is in the range 2–3 with a lower value observed for lipid membranes; while $k_0^{(\alpha)}$ varies from case to case, being known explicitly for uniform fractal spaces.¹² This type of relaxation behavior may vastly complicate its removal from PDS data; therefore, low values of $\bar{C}_{\text{loc}}^{(\alpha)}$ are desirable.

20.7.4 Relaxation Effects in PDS

Unlike ID, which in principle is a coherent process, there are relaxation mechanisms that impose a limit to what PDS can accomplish in terms of distance measurements. The distance range and resolution is limited by the achievable duration t_m of dipolar evolution that one can record for a given sample. Typically, for biomolecules, a simple-exponential phase-relaxation law is observed with T_m 's of the order 1–2 μs . When relaxation is relatively slower, e.g., for solvent-exposed spin labels, the nuclear spin-diffusion relaxation mechanism dominates for a longer time, leading to a signal decay, which in aqueous solutions is described by a stretched exponential such as $\exp[-(2t_m/T_m)^\kappa]$, with κ in the range 1.5–3 and a phase memory time $T_m \approx 4 \mu\text{s}$. This sets a limit of about 5 nm to the upper range of distances that can be measured accurately. Resolution for longer distances require solvent deuteration or in critical

cases could include deuteration of the biomolecule as well,^{100,102,104} virtually eliminating the effects of nuclear spin diffusion. It is well known that a CPMG pulse sequence is efficient in suppression of such spin diffusion processes; hence, this is relevant to PDS. As single-resonance methods described in this article are based on RE, there is a partial suppression of nuclear spin diffusion in them. This also was realized in the form of the DQ-filtered RE pulse sequence.⁶⁹ A more efficient approach, however, was undertaken for DEER, where multipulse CPMG-based PDS pulse sequences were applied for deeper suppression of spin diffusion.²⁴

20.7.5 Relaxation in Single- and Double-resonance

As in double resonance the detection pulse sequence has its pulse fixed, the only time-dependent signal decay is caused by ID due to spins B, thus yielding the background slope. (The methods that use long coherence storage time T , experience effects of spectral diffusion.⁴⁴) The echo signal, however, decays due to phase relaxation as $\exp[-(2t_m/T_m)^\kappa]$. The behavior is different for single resonance, where the need to vary the duration of refocusing sequences (see Section 20.2.6) for $\kappa \neq 1$ produces relaxation decay that has an effect on the dipolar signal shape given by

$$R(t_x) = \exp[-((t_m - t_x)^\kappa + (t_m + t_x)^\kappa)/T_m^\kappa] \quad (20.39)$$

Such behavior is evident in Figure 20.8(a). For $t_x = 0$, equation (20.39) yields $\exp(-2t_m^\kappa/T_m^\kappa)$, which corresponds to a longer $T'_m = 2^{1-1/\kappa} T_m$. In single-resonance pulse sequences, the t_x dependence in equation (20.39) favors the signal amplitude at small t_x , which de facto introduces signal windowing vs t_x . Signal acquisition as a function of t_m at condition $t_x = 0$ was used to extend the evolution in the DQ-filtered RE pulse sequence.⁶⁹

20.8 CONCLUSIONS

A variety of modern PDS methods implemented at several frequencies are available today, allowing one to find the best conditions for accurate distance measurement as well as improved distance resolution and orientation selection. Although many new PDS methods are being developed, double- and single-resonance

methods constitute the two major groups, which are not always clearly distinguishable. The pure, coherent, single-resonance techniques described in this article are making an increasing contribution as pulse technology rapidly progresses. For nearly the past two decades, DQC with hard pulses was a 'gold standard' for this class of techniques, as it provides high-quality distance data at high spin sensitivity, while at the same time allowing robust implementation at several convenient working frequencies. Recent improvements in SIFTER based on broadband adiabatic pulses are helping to develop this potentially useful and sensitive technique. This includes adding 2D-SIFTER experiments to the methods for the study of orientational correlations represented by 2D-DQC. This extends the methods to look at orientations, which also include HFHF DEER^{38,101,105,106} and RIDME.^{38,101}

So far, the standard four-pulse DEER method and its recent extensions such as multiple-pulse dipolar refocusing CPMG-type DEER^{24,107,108} are the mainstay techniques as a matter of application flexibility, modest requirements of peak power, and reach to long distances. However, there are an increasing number of cases where DQC, SIFTER, or RIDME are better suited or may have no alternatives. For DQC and SIFTER, this particularly includes cases such as trityl label, especially in liquid solutions,⁶⁸ radical cofactors, low-concentration samples where sensitivity is a key issue, whereas broad spectra such as those of transition metal ions may benefit from RIDME, which otherwise is not an alternative to DQC or DEER. For nearly two decades, we have used DEER and DQC techniques, implemented at K_u band for high sensitivity, which has enabled many studies on important biological systems, and we have a positive outlook into the future use of these PDS techniques. We have emphasized DQC of the single-resonance methods, as with current technology, it is the most effective in avoiding unwanted signals. While there was a large effort to increase the sensitivity of PDS methods, a minimal level of signal artifacts may be even more important than modest SNR improvements paid for by the loss of signal fidelity. Relatively small signal artifacts may contribute a more serious impediment to extraction of distance information from the dipolar evolution traces than a moderate loss of SNR, as evidenced by the reconstruction of simulated vs experimental data.^{78,109}

Nevertheless, spin sensitivity is of utmost importance in PDS and it usually is studied for nitroxides, in particular using MTSL as the main spin label.^{24,110}

Furthermore, we mention new methods of signal processing the PDS data, which are an additional approach to significantly improving the SNR of the experiment, somewhat relaxing the need of high SNR.^{109,111} However, today, there is a large and increasing variety of spin labels based on nitroxides, trityls, photoexcited states, cofactors, or metal ions, both endo- and exogenous, as well as a plurality of vastly different PDS methods.^{82,97,106,112} The particular experiment or spin label often benefits from using the most suitable technique, and single-resonance methods such as DQC and SIFTER and others described here will play increasingly valuable roles.

ACKNOWLEDGMENTS

The authors acknowledge NIH NIGMS Grant P41 GM103521 to ACERT National Biomedical Center for Advanced EPR Technology. The authors are grateful to Dr. Elka R. Georgieva for providing spin-labeled T4-lysozyme protein samples that enabled us to obtain model DQC and SQC data shown in this chapter. The authors are thankful to our multiple collaborators and group members that over the course of 15 years made a great contribution to the development of biomolecular PDS spectroscopy at ACERT. In particular the efforts of Brian R. Crane, Elka R. Georgieva, David Eliezer, Betty J. Gaffney, Hassane S. Mchaourab, Olga Boudker, Sang-Youn Park, Jaya Bhatnagar, Yun-Wej Chiang, Wayne L. Hubbell, Samuel E. Butcher, Dale Edmondson, Anup Upadhyay, Shaogeng Tang, Scott D. Emr, Charles P. Scholes, Ria Sircar, Dipanjan Samanta, Gregory E. Merz, Kent Kirshenbaum, Boris D. Dzikovski, Yeon-Kyun Shin, Jiansong Tong, Vladimir M. Grigoryants, Trudy F. Ramlall, Zhongyu Yang, Alexandrine M. Crane, Songi Han, Neil A. Eschmann, Sushil K. Misra, Aaron T. Fafarman, Michael V. Airola, David E. Budil, Michael G. Malkowski, Benjamin J. Orlando, Elizabeth D. Getzoff, Nattakan Sukomon are highly appreciated.

REFERENCES

1. A. M. Raitsimring and K. M. Salikhov, *Bull. Magn. Reson.*, 1985, **7**, 184.
2. L. Kevan and R. N. Schwartz, in *Time Domain Electron Spin Resonance*, eds L. Kevan and R. N. Schwartz, John Wiley & Sons, Inc.: New York, 1979.
3. A. Raitsimring, in *Biological Magnetic Resonance*, eds L. J. Berliner, G. R. Eaton and S. S. Eaton, Kluwer Academic: New York, 2000, Vol. 19, p 385.
4. A. Abragam, *The Principles of Nuclear Magnetism*, Clarendon Press: Oxford, 1961.
5. J. Klauder and P. Anderson, *Phys. Rev.*, 1962, **125**, 912.
6. V. F. Yudanov, K. M. Salikhov, G. M. Zhidormirov, and Y. D. Tsvetkov, *Theor. Exp. Chem.*, 1972, **5**, 451.
7. S. A. Dikanov and Y. Tsvetkov, *Electron Spin Echo Envelope Modulation (ESEEM) Spectroscopy*, Taylor & Francis: London, 1992.
8. A. Schweiger and G. Jeschke, *Principles of Pulse Electron Paramagnetic Resonance*, Oxford University Press: Oxford, 2001.
9. W. B. Mims, *Phys. Rev. B Solid State*, 1972, **5**, 2409.
10. M. Emshwiller, E. L. Hahn, and D. Kaplan, *Phys. Rev.*, 1960, **118**, 414.
11. A. D. Milov, K. M. Salikhov, and M. D. Shirov, *Sov. Phys. Solid State*, 1981, **23**, 565.
12. A. D. Milov and Y. D. Tsvetkov, *Appl. Magn. Reson.*, 1997, **12**, 495.
13. G. E. Merz, P. P. Borbat, A. J. Pratt, E. D. Getzoff, J. H. Freed, and B. R. Crane, *Biophys. J.*, 2014, **107**, 1669.
14. P. P. Borbat and J. H. Freed, in *Two-Component Signaling Systems*, Pt B, eds M. I. Simon, B. R. Crane and A. Crane, Elsevier Academic Press Inc: San Diego, 2007, Vol. 423, p 52.
15. A. V. Astashkin and A. Kawamori, in *Biophysical Techniques in Photosynthesis*, eds T. Aartsma and J. Matysik, Springer: Dordrecht, Netherlands, 2008, Vol. 2, p 325.
16. M. Pannier, S. Veit, A. Godt, G. Jeschke, and H. W. Spiess, *J. Magn. Reson.*, 2000, **142**, 331.
17. L. J. Berliner, G. R. Eaton, and S. S. Eaton, *Distance Measurements in Biological Systems by EPR*, Kluwer Academic: New York, 2000.
18. R. E. Martin, M. Pannier, F. Diederich, V. Gramlich, M. Hubrich, and H. W. Spiess, *Angew. Chem. Int. Ed.*, 1998, **37**, 2834.
19. S. Saxena and J. H. Freed, *J. Chem. Phys.*, 1997, **107**, 1317.
20. P. P. Borbat and J. H. Freed, *Chem. Phys. Lett.*, 1999, **313**, 145.
21. P. P. Borbat and J. H. Freed, in *Biological Magnetic Resonance*, eds L. J. Berliner, G. R. Eaton and S.

- S. Eaton, Academic/Plenum Publishers: New York, 2000, Vol. 19, p 385.
22. P. P. Borbat and J. H. Freed, in *Structural Information from Spin-Labels and Intrinsic Paramagnetic Centres in the Biosciences*, eds C. R. Timmel and J. R. Harmer, Springer-Verlag: Berlin, 2014, Vol. 152, p 1.
 23. G. Jeschke, M. Pannier, A. Godt, and H. W. Spiess, *Chem. Phys. Lett.*, 2000, **331**, 243.
 24. P. P. Borbat, E. R. Georgieva, and J. H. Freed, *J. Phys. Chem. Lett.*, 2013, **4**, 170.
 25. G. Jeschke, A. Bender, H. Paulsen, H. Zimmermann, and A. Godt, *J. Magn. Reson.*, 2004, **169**, 1.
 26. S. Milikisyants, F. Scarpelli, M. G. Finiguerra, M. Ubbink, and M. Huber, *J. Magn. Reson.*, 2009, **201**, 48.
 27. L. V. Kulik, Y. A. Grishin, S. A. Dzuba, I. A. Grigoryev, S. V. Klyatskaya, S. F. Vasilevsky, and Y. D. Tsvetkov, *J. Magn. Reson.*, 2002, **157**, 61.
 28. S. Razzaghi, M. Qi, A. I. Nalepa, A. Godt, G. Jeschke, A. Savitsky, and M. Yulikov, *J. Phys. Chem. Lett.*, 2014, **5**, 3970.
 29. D. Abdullin, F. Duthie, A. Meyer, E. S. Muller, G. Hagelueken, and O. Schiemann, *J. Phys. Chem. B*, 2015, **119**, 13534.
 30. A. Collauto, V. Frydman, M. D. Lee, E. H. Abdelkader, A. Feintuch, J. D. Swarbrick, B. Graham, G. Otting, and D. Goldfarb, *Phys. Chem. Chem. Phys.*, 2016, **18**, 19037.
 31. P. P. Borbat, H. S. Mchaourab, and J. H. Freed, *J. Am. Chem. Soc.*, 2002, **124**, 5304.
 32. S.-Y. Park, P. P. Borbat, G. Gonzalez-Bonet, J. Bhatnagar, A. M. Pollard, J. H. Freed, A. M. Bilwes, and B. R. Crane, *Nat. Struct. Mol. Biol.*, 2006, **13**, 400.
 33. G. Jeschke, C. Wegener, M. Nietschke, H. Jung, and H.-J. Steinhoff, *Biophys. J.*, 2004, **86**, 2551.
 34. B. G. Dzikovski, P. P. Borbat, and J. H. Freed, *Biophys. J.*, 2004, **87**, 3504.
 35. O. Schiemann, N. Piton, Y. G. Mu, G. Stock, J. W. Engels, and T. F. Prisner, *J. Am. Chem. Soc.*, 2004, **126**, 5722.
 36. P. A. S. Cruickshank, D. R. Bolton, D. A. Robertson, R. I. Hunter, R. J. Wylde, and G. M. Smith, *Rev. Sci. Instrum.*, 2009, **80**, 103102.
 37. G. W. Reginsson, R. I. Hunter, P. A. S. Cruickshank, D. R. Bolton, S. T. Sigurdsson, G. M. Smith, and O. Schiemann, *J. Magn. Reson.*, 2012, **216**, 175.
 38. K. Möbius and A. Savitsky, *High-Field EPR Spectroscopy on Proteins and Their Model Systems: Characterization of Transient Paramagnetic States*, Royal Society of Chemistry: Cambridge, 2009.
 39. P. E. Spindler, P. Schops, A. M. Bowen, B. Endeward, and T. F. Prisner, *eMagRes*, 2016, **5**, 1477.
 40. A. Doll, M. Qi, A. Godt, and G. Jeschke, *J. Magn. Reson.*, 2016, **273**, 73.
 41. A. Doll, M. A. Qi, S. Pribitzer, N. Wili, M. Yulikov, A. Godt, and G. Jeschke, *Phys. Chem. Chem. Phys.*, 2015, **17**, 7334.
 42. C. P. Slichter, *Principles of Magnetic Resonance*, Springer-Verlag: Berlin, 1990, p 248.
 43. C. Hintze, D. Bucker, S. D. Kohler, G. Jeschke, and M. Drescher, *J. Phys. Chem. Lett.*, 2016, **7**, 2204.
 44. A. V. Astashkin, in *Electron Paramagnetic Resonance Investigations of Biological Systems by Using Spin Labels, Spin Probes, and Intrinsic Metal Ions*, Pt A, eds P. Z. Qin and K. Warncke, 2015, Vol. 563, p 251.
 45. R. R. Ernst et al., *Principles of Nuclear Magnetic Resonance in One and Two Dimensions*, Clarendon Press: Oxford [Oxfordshire], 1987.
 46. O. W. Sorensen, G. W. Eich, M. H. Levitt, G. Bodenhausen, and R. R. Ernst, *Prog. Nucl. Magn. Reson. Spectrosc.*, 1983, **16**, 163.
 47. J. Cavanagh, *Protein NMR Spectroscopy: Principles and Practice*, Academic Press, 1996.
 48. C. P. Slichter, *Principles of Magnetic Resonance*, 3rd edn, Springer-Verlag: Berlin-Heidelberg-New-York, 1990.
 49. G. E. Pake, *J. Chem. Phys.*, 1948, **16**, 327.
 50. H. W. Spiess and K. Schmidt-Rohr, *Multidimensional Solid-State NMR and Polymers*, Academic Press: London, 1994.
 51. A. D. Bain, D. A. Fletcher, and P. Hazendonk, *Concepts Magn. Reson.*, 1998, **10**, 85.
 52. J. Shriver, *Concepts Magn. Reson.*, 1992, **4**, 1.
 53. M. H. Levitt, *eMagRes*, John Wiley & Sons, Ltd: Chichester, 2007.
 54. J. H. Freed, *Annu. Rev. Phys. Chem.*, 2000, **51**, 655.
 55. J. H. Freed, *Annu. Rev. Phys. Chem.*, 1972, **23**, 265.
 56. M. H. Levitt, *Pulse Methods in 1D & 2D Liquid-Phase NMR*, Academic Press: San Diego, 1988, p 111.
 57. M. H. Levitt, *Spin Dynamics: Basics of Nuclear Magnetic Resonance*, John Wiley & Sons, Ltd: Chichester, 2008.

58. M. Di Valentin, M. Albertini, E. Zurlo, M. Gobbo, and D. Carbonera, *J. Am. Chem. Soc.*, 2014, **136**, 6582.
59. S. A. Dzuba and A. Hoff, in *Biological Magnetic Resonance*, eds L. J. Berliner, G. R. Eaton and S. S. Eaton, Academic/Plenum Publishers: New York, 2000, Vol. 19, p 569.
60. G. Jeschke, M. Pannier, and H. W. Spiess, in *Distance Measurements in Biological Systems by EPR*, eds L. J. Berliner, G. R. Eaton and S. S. Eaton, Springer: Boston, MA, 2002, p 493.
61. J. G. Powles and P. Mansfield, *Phys. Lett.*, 1962, **2**, 58.
62. P. P. Borbat, R. H. Crepeau, and J. H. Freed, *J. Magn. Reson.*, 1997, **127**, 155.
63. B. J. Gaffney, M. D. Bradshaw, S. D. Frausto, F. Y. Wu, J. H. Freed, and P. Borbat, *Biophys. J.*, 2012, **103**, 2134.
64. C. E. Tait and S. Stoll, *Phys. Chem. Chem. Phys.*, 2016, **18**, 18470.
65. S. K. Misra, P. P. Borbat, and J. H. Freed, *Appl. Magn. Reson.*, 2009, **36**, 237.
66. A. T. Fafarman, P. P. Borbat, J. H. Freed, and K. Kirshenbaum, *Chem. Commun.*, 2007, 377.
67. M. Bennati, J. H. Robblee, V. Mugnaini, J. Stubbe, J. H. Freed, and P. Borbat, *J. Am. Chem. Soc.*, 2005, **127**, 15014.
68. Z. Y. Yang, Y. P. Liu, P. Borbat, J. L. Zweier, J. H. Freed, and W. L. Hubbell, *J. Am. Chem. Soc.*, 2012, **134**, 9950.
69. P. P. Borbat, J. H. Davis, S. E. Butcher, and J. H. Freed, *J. Am. Chem. Soc.*, 2004, **126**, 7746.
70. M. Huber, M. Lindgren, P. Hammarstrom, L.-G. Martensson, U. Carlsson, G. R. Eaton, and S. S. Eaton, *Biophys. Chem.*, 2001, **94**, 245.
71. A. D. Milov, K. M. Salikhov, and Y. D. Tsvetkov, *Fiz. Tverd. Tela*, 1973, **15**, 1187.
72. K. N. Hu, C. Song, H. H. Yu, T. M. Swager, and R. G. Griffin, *J. Chem. Phys.*, 2008, **128**.
73. P. Schoeps, P. E. Spindler, A. Marko, and T. F. Prisner, *J. Magn. Reson.*, 2015, **250**, 55.
74. S. M. Islam, R. A. Stein, H. S. Mchaourab, and B. Roux, *J. Phys. Chem. B*, 2013, **117**, 4740.
75. E. R. Georgieva, A. S. Roy, V. M. Grigoryants, P. P. Borbat, K. A. Earle, C. P. Scholes, and J. H. Freed, *J. Magn. Reson.*, 2012, **216**, 69.
76. M. Lindgren, G. R. Eaton, S. S. Eaton, B.-H. Jonsson, P. Hammarstrom, M. Svensson, and U. Carlsson, *J. Chem. Soc. Perkin Trans.*, 1997, **2**, 2549.
77. A. D. Milov, K. M. Salikhov, and Y. D. Tsvetkov, *Sov. Phys. Solid State*, 1973, **15**, 802.
78. Y.-W. Chiang, P. P. Borbat, and J. H. Freed, *J. Magn. Reson.*, 2005, **172**, 279.
79. S. Ruthstein, M. Ji, B. K. Shin, and S. Saxena, *J. Magn. Reson.*, 2015, **257**, 45.
80. J. Jeener and P. Broekaert, *Phys. Rev.*, 1967, **157**, 232.
81. G. Y. Shevelev, O. A. Krumkacheva, A. A. Lomzov, A. A. Kuzhelev, O. Y. Rogozhnikova, D. V. Trukhin, T. I. Troitskaya, V. M. Tormyshev, M. V. Fedin, D. V. Pyshnyi, and E. G. Bagryanskaya, *J. Am. Chem. Soc.*, 2014, **136**, 9874.
82. D. Akhmetzyanov, P. Schops, A. Marko, N. C. Kujir, S. T. Sigurdsson, and T. F. Prisner, *Phys. Chem. Chem. Phys.*, 2015, **17**, 24446.
83. G. Jeschke, V. Chechik, P. Ionita, A. Godt, H. Zimmermann, J. Banham, C. R. Timmel, D. Hilger, and H. Jung, *Appl. Magn. Reson.*, 2006, **30**, 473.
84. A. Doll and G. Jeschke, *Phys. Chem. Chem. Phys.*, 2016, **18**, 23111.
85. J. M. Bohlen and G. Bodenhausen, *J. Magn. Reson. Ser. A*, 1993, **102**, 293.
86. M. Bonora, J. Becker, and S. Saxena, *J. Magn. Reson.*, 2004, **170**, 278.
87. A. J. Hoff, P. Gast, S. A. Dzuba, C. R. Timmel, C. E. Fursman, and P. J. Hore, *Spectrochim. Acta Mol. Biomol. Spectrosc.*, 1998, **54**, 2283.
88. J. Tang, M. C. Thurnauer, and J. R. Norris, *Chem. Phys. Lett.*, 1994, **219**, 283.
89. A. Marko, V. Denysenkov, and T. F. Prisner, *Mol. Phys.*, 2013, **111**, 2834.
90. R. R. Mett, J. W. Sidabras, I. S. Golovina, and J. S. Hyde, *Rev. Sci. Instrum.*, 2008, **79**, Article number: 094702.
91. R. R. Mett, J. W. Sidabras, and J. S. Hyde, *Appl. Magn. Reson.*, 2007, **31**, 573.
92. J. Forrer, I. Garcia-Rubio, R. Schuhmam, R. Tschaggelar, and J. Harmer, *J. Magn. Reson.*, 2008, **190**, 280.
93. S. Pfenninger, J. Forrer, A. Schweiger, and T. Weiland, *Rev. Sci. Instrum.*, 1988, **59**, 752.
94. V. V. Kurshev, A. M. Raitsimring, and Y. D. Tsvetkov, *J. Magn. Reson.*, 1989, **81**, 441.

95. L. V. Kulik, S. A. Dzuba, I. A. Grigoryev, and Y. D. Tsvetkov, *Chem. Phys. Lett.*, 2001, **343**, 315.
96. A. Meyer and O. Schiemann, *J. Phys. Chem. A*, 2016, **120**, 3463.
97. A. M. Bowen, C. E. Tait, C. R. Timmel, and J. R. Harmer, in *Structural Information from Spin-Labels and Intrinsic Paramagnetic Centres in the Biosciences*, eds C. R. Timmel and J. R. Harmer, Springer: Berlin, 2013, p 283.
98. V. V. Kurshev and T. Ichikawa, *J. Magn. Reson.*, 1992, **96**, 563.
99. A. A. Nevzorov and J. H. Freed, *J. Chem. Phys.*, 2001, **115**, 2401.
100. E. R. Georgieva, T. F. Ramlall, P. P. Borbat, J. H. Freed, and D. Eliezer, *J. Biol. Chem.*, 2010, **285**, 28261.
101. A. Savitsky, J. Niklas, J. H. Golbeck, K. Mobius, and W. Lubitz, *J. Phys. Chem. B*, 2013, **117**, 11184.
102. T. Schmidt, M. A. Walti, J. L. Baber, E. J. Hustedt, and G. M. Clore, *Angew. Chem. Int. Ed.*, 2016, **55**, 15905.
103. W. S. Warren, *J. Chem. Phys.*, 1984, **81**, 5437.
104. W. Richard, A. Bowman, E. Sozudogru, H. El-Mkami, T. Owen-Hughes, and D. G. Norman, *J. Magn. Reson.*, 2010, **207**, 164.
105. C. L. Motion, J. E. Lovett, S. Bell, S. L. Cassidy, P. A. S. Cruickshank, D. R. Bolton, R. I. Hunter, H. El Mkami, S. Van Doorslaer, and G. M. Smith, *J. Phys. Chem. Lett.*, 2016, **7**, 1411.
106. D. Goldfarb, in *Structural Information from Spin-Labels and Intrinsic Paramagnetic Centres in the Biosciences*, eds C. R. Timmel and J. R. Harmer, Springer: Heidelberg, 2013, p 163.
107. P. E. Spindler, I. Waclawska, B. Endeward, J. Plackrneyer, C. Ziegler, and T. F. Prisner, *J. Phys. Chem. Lett.*, 2015, **6**, 4331.
108. J. M. Soetbeer, *Dynamical Decoupling in Distance Measurements by Double Electron–electron Resonance*, Springer Spektrum: Wiesbaden, 2016.
109. M. Srivastava, E. R. Georgieva, and J. H. Freed, *J. Phys. Chem. A*, 2017, **121**, 2452.
110. R. Tschaggelar, B. Kasumaj, M. G. Santangelo, J. Forrer, P. Leger, H. Dube, F. Diederich, J. Harmer, R. Schuhmann, I. Garcia-Rubio, and G. Jeschke, *J. Magn. Reson.*, 2009, **200**, 81.
111. M. Srivastava, C. L. Anderson, and J. H. Freed, *IEEE Access*, 2016, **4**, 3862.
112. Z. Y. Yang, M. Ji, T. F. Cunningham, and S. Saxena, in *Electron Paramagnetic Resonance Investigations of Biological Systems by Using Spin Labels, Spin Probes, and Intrinsic Metal Ions, Pt A*, eds P. Z. Qin and K. Warncke, 2015, Vol. 563, p 459.